# Chemical reactions induced by localized light and their application to metal nanofabrication

(局在した光により誘起される化学反応と

その金属ナノ加工への応用)

March 2023

Graduate School of Natural Science and Technology

(Doctor's Course)

OKAYAMA UNIVERSITY

Yuki Takeuchi

# Contents

# Abstract

The color of metal nanostructures is different from that in the bulk state. The difference in color is caused by varying the optical property because free electrons in the metal resonate with electric fields of incident light at the specific wavelength and the light is localized at the metallic nanosurface. The phenomenon is well-known as "localized surface plasmon resonance" (LSPR). Lots of applications using the LSPR have been expected. Among them, surface-enhanced Raman scattering (SERS) spectroscopy, which is the technique to enhance the intensity of the Raman scattering, has been paid attention to and can overcome drawbacks of conventional Raman scattering spectroscopy. During the research for application of the metal nanostructures to spectroscopy, it has emerged that measured molecules on the metal are chemically transformed by LSPR, which is currently called plasmon-induced chemical reactions. In recent years, it has been demonstrated that the metal nanostructures are applied to photochemical reaction fields. However, the use of metal nanostructures has progressed slowly because lots of unrevealed things are remained for the plasmon-induced chemical reactions. In this dissertation, I investigated the reactivity of organic compounds at metallic nanosurface under light illumination, and the incident light and material dependence of the plasmon-induced chemical reaction. In addition, I conceived that the reaction would be applicable to metal nanofabrication, therefore linkages of gold nanoparticles (AuNPs) were demonstrated.

In Chapter 1, LSPR and localization effect of incident light on a metallic nanosurface are described, and the SERS spectroscopy is also introduced. Furthermore, plasmon-induced chemical reactions of molecules on the metal nanosurface during the measurement of SERS spectra are explained.

In Chapter 2, the reactivity of silver nanoparticles (AgNPs) was investigated using SERS monitoring of plasmon-induced chemical reactions. First, SERS active substrates were prepared by self-assembling AgNPs to the two-dimensional (2D) arrays and transferring them onto glass substrates. To evaluate the reactivity of the AgNP 2D array, SERS spectra of *para*-toluenethiol (*p*-TT) and 1-butanethiol (1-BT) were measured using the substrates. In those spectra, it was confirmed that new peaks appeared as the incident light intensity increased. Furthermore, assignments of the peaks indicate that *p*-TT and 1-

BT were oxidized during the SERS measurements. The spectra of the products after the reactions suggested that the oxidation proceeded by the dissociation and radicalization of oxygen on the surface of AgNPs. The incident light dependence and material dependence of the plasmon-induced chemical reaction were also described in this chapter. From the SERS monitoring of the chemical reaction of *p*-aminothiophenol (*p*-ATP) to *p,p'*-dimercaptoazobenzene (DMAB) at different conditions of incident light, it was concluded that the shorter excitation wavelength or higher intensity of incident light were favorable for the chemical reaction. In addition, the material dependence of the reaction from *p*-ATP to DMAB was discussed by comparing the reactivity between gold and silver, which are frequently used as plasmonic materials. As a conclusion, it was found that the photochemical reaction rate at silver was higher than the rate at gold.

In Chapter 3, linkages of gold nanoparticles (AuNPs) by light illumination were demonstrated as the one example for application of the reaction to metal nanofabrication. The light illumination of AuNPs fixing substrates in the gold ion solution were performed and linkages of the AuNPs were confirmed by comparing the scanning electron microscope (SEM) images before and after the light illumination. Furthermore, it was confirmed that the AuNPs were not linked when either gold ion or light illumination lacked, implying the AuNPs bridged by gold generated through the reduction of gold ions under the light illumination. Electric field distribution on the AuNPs was also simulated using electromagnetic field analysis methods to investigate the origin of the nanoparticle linking process predicted by the SEM images. The simulation results implied that the nanoparticle linking process was determined by localization spots of light on the metallic nanosurface via plasmons. In conclusion, the linkages of AuNPs fixed on glass substrates under the light illumination was caused by the localized light at gold nanosurface, which was plasmon-induced reduction of gold ions.

In Chapter 4, I describe the linkages of AuNPs dispersed in solution by the light illumination. First, AuNP oligomer solutions were prepared by adding salt and ethanol to AuNP monomer aqueous solutions. After adding gold ions to the oligomer solutions, the solutions were then illuminated to link the oligomers. The linked oligomers were observed using a high-resolution transmission electron microscopy (TEM). The TEM images revealed that the illuminated AuNPs were linked, and the linkage part was grown

as increasing the illumination time by comparing the images at the different illumination times. Energy dispersive X-ray spectroscopy also revealed that the linkage part was composed of gold. It indicated that the AuNPs dispersed in the solution were linked by gold generated from the gold ion reduction induced by light localized at gold nanosurface via LSPR. The transition of optical property was confirmed by measuring the extinction spectrum. It was observed that the spectral shapes of AuNP oligomer solutions were transformed after the light illumination. Theoretical methods confirmed that the transformation of the shape was caused by the linkages of AuNP oligomers and the growth of the linkage parts. In conclusion, the proposed method to link AuNPs provided the AuNPs which resonate with near-infrared (NIR) light and facilitated tuning the resonance wavelength from visible to NIR regions.

In Chapter 5, obtained all results were summarized as a general conclusion.

# Chapter 1
# General introduction

## 1.1  Metal nanostructures exhibiting unique optical properties

### 1.1.1  Localized surface plasmon resonance

Nanomaterials exhibiting unique physical and chemical properties have been focused on technological advancements. Current nanomaterials can be classified into four material-based categories, (i) carbon-based nanomaterials, (ii) inorganic-based materials, (iii) organic-based materials and (iv) composite-based materials.[1] For instance, representative nanomaterials graphene and carbon nanotubes are included in carbon-based materials.[2,3] In inorganic-based nanomaterials, metal, and metal oxide nanoparticles such as gold nanoparticle (AuNP) and titanium oxide are well known. On the other hand, micelles, liposomes, and polymer nanoparticles are included under the organic-based nanomaterial category. The composite-based nanomaterials are multi-phase nanoparticles and nanostructures that either combine nanoparticles with other nanoparticles or nanoparticles combined with larger or with bulk-type materials or more complicated structures, such as metal-organic frameworks.

Among them, the metallic nanostructures such as AuNPs exhibit totally different optical properties from those in bulk. Figure 1-1(a) shows gold in bulk state and AuNP aqueous solution. While the bulk gold shows the typical color of gold and reflects light, the color of AuNP aqueous solution is reddish. The color difference indicates that the optical property of gold changed by decreasing the size of structures to nanometers scale. It is well known that the transition of optical properties is caused by the interaction between free electrons in those metals and the electric field of incident light. When the metallic nanostructures are illuminated by light, the free electrons respond to the electric field of the light. At certain frequencies of light, the free electrons collectively oscillate with the electric fields of the light, in other words, resonance between free electrons and the light are caused as shown in Fig. 1-1(b). The resonance leads to the transition of the optical property, and it is known as localized surface plasmon resonance (LSPR).[4-6]

8
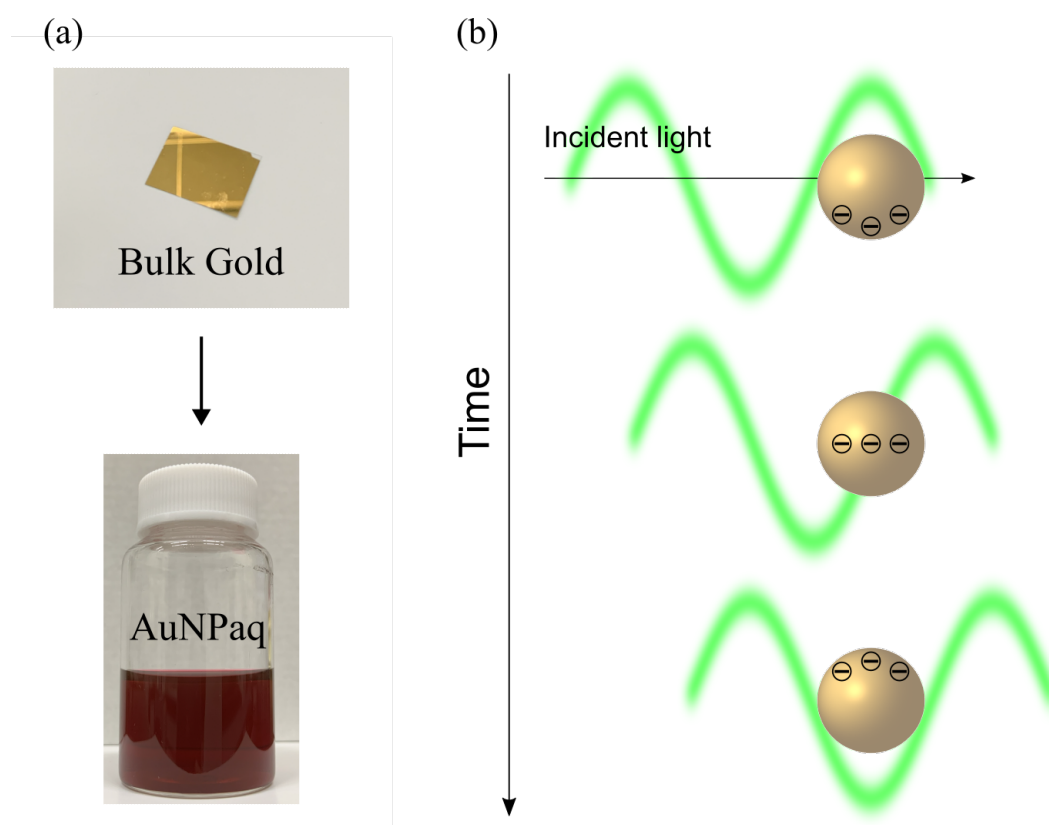
Figure 1-1. (a) Photographs of bulk gold and AuNP aqueous solution. (b) Schematic illustration of localized surface plasmon resonance, where collective oscillation of free electrons is excited by electric fields of incident light.

### 1.1.2 Tuning resonance of the metal nanostructures

The resonance wavelength of the metal nanostructure is determined by the scale, geometry, and surrounding media (Fig.1-2).[7,8] A wide variety of methods to fabricate or tailor the geometry have been proposed for tuning the resonance wavelengths in terms of both bottom-up and top-down approaches. In the top-down approach, the plasmonic patterns were engraved on the metal films using electron beam lithography.[9,10]
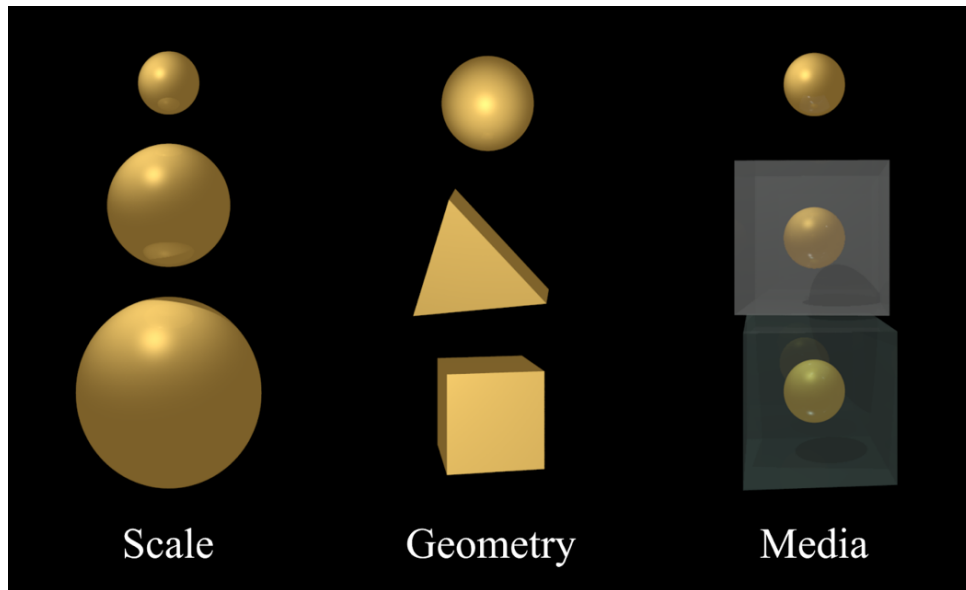


Figure 1-2. Factors affecting the resonance wavelength of metal nanostructure.

The fabrication methods of metal nanostructures using not only the electron beam but also light have been proposed. Figure 1-3(a) shows scanning electron microscope (SEM) images of free-standing silver pillars on a cover slip fabricated by the multi-photon induced metal ion reductions.[11] In the method, multi-photon reduction of silver ions was achieved only at the focusing spot of incident laser, where a femtosecond laser was used as an external stimulus. Scanning the focusing spot enabled fabrication of three-dimensional structures with arbitrary geometry such as free-standing three-dimensional silver pyramids (Fig.1-3b).
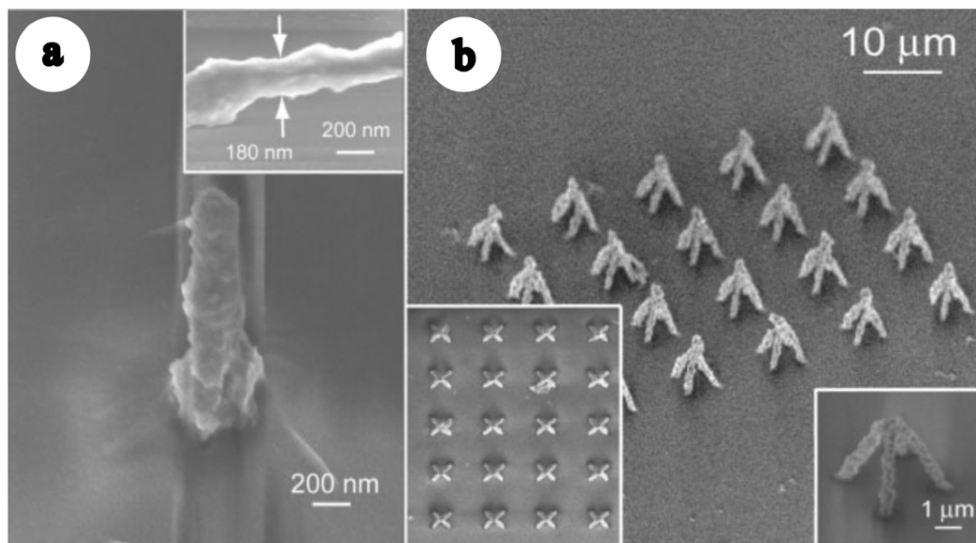
Figure 1-3. SEM images of silver nanostructures fabricated by light illumination. (a) Free-standing silver pillar. (b) Free-standing three-dimensional silver pyramids. The inset on the left is a top view of the silver-pyramid array. The inset on the right is a close-up view of the silver pyramid.

Chemical approach is one of the major methods, which is a kind of bottom-up approach for mass production. In the chemical approach, metal nanoseeds are generated during the reduction of metal ions in the presence of reductants and the seeds are self-grown due to the reductions, resulting in both isotropic and anisotropic nanoparticles. For instance, it was reported that rod-like AuNPs exhibiting two resonances were prepared by seed mediated growth method using cetyltrimethylammonium bromide, which is a surfactant to protect the growth at the side of Au seeds. The two resonances were formed because of the anisotropic structure. The resonance at shorter wavelength regions is derived from oscillation of free electrons according to the short axis, known as transverse mode. On the other hand, the resonance at longer wavelength regions is derived from electron oscillation along the long axis and is called longitudinal mode. Figure 1-4 shows the transmission electron microscope (TEM) images of gold nanorods (AuNRs) resonating with 700, 760, 790, 880, 1130, and 1250 nm.[12] The correlation between each geometry and resonance indicated that resonance wavelength of AuNRs were dependent on the geometry, particularly the length of both short and long axes. It was further reported that the resonance wavelength was determined by the ratio between length of long and short axes, which is aspect ratio.[13] In addition to the rod shape, the methods to prepare various

geometrical nanoparticles were proposed to tune those resonances (*e.g.,* triangle, cube, star).[14-16]
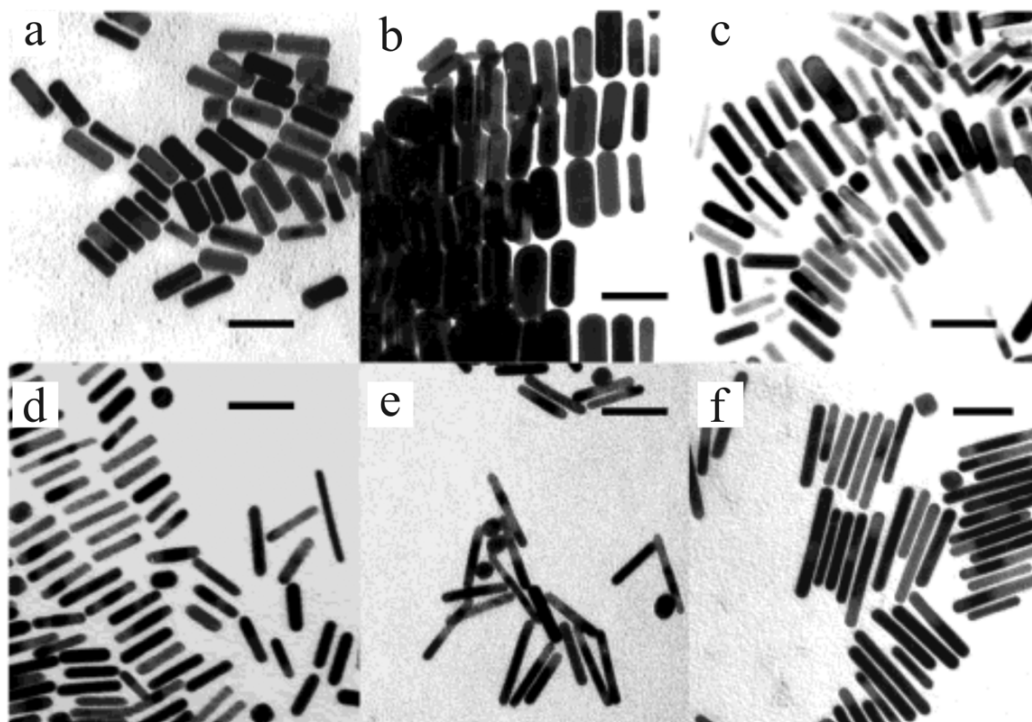


Figure 1-4. TEM images of AuNRs with plasmon band energies at (a) 700, (b) 760, (c) 790, (d) 880, (e) 1130, and (f) 1250 nm.

The resonance of metal nanoparticles is also shifted by varying the distance between metal nanoparticles. Figure 1-5(a) shows the plot of wavelength shifts according to the gap distance between Au elliptical particles obtained by calculated or experimentally measured.[17] The shifts and inter-particle distances were normalized by the peak wavelengths and the lengths of short axes, respectively. In the plot, it seems that the peak is shifted to longer wavelength regions when the gap distance is short. The resonance shift is caused by the hybridization of the LSPR mode in each particle. The light illumination of metal nanoparticles leads to the collective oscillation of the free electrons in the metal and thus, a dipole is generated. When the metal nanoparticle is adjacent to the other metal particles, the dipoles interact with each other and the LSPRs are hybridized as well as the molecular orbitals.[18] By the hybridization of LSPRs, the energy state is split into more than two states. Figure 1-5(b) represents the energy level of LSPR excited in a metal

particle and the split due to the hybridization when the particle is adjacent to the other particle, in other words, a metal nanoparticle dimer is formed. In the energy diagram, the state of LSPR is split into two states. The lower energy level is formed when the direction of two dipoles is corresponded, called bonding dipole mode. On the other hand, the opposite direction of dipoles leads to formation of the higher energy level, which is known as antibonding mode. Generally, because the antibonding mode is excited through forbidden transition by light illumination, the spectrum shows the peak derived from only bonding mode. Therefore, the peak shift to longer wavelength regions is observed in the spectrum. By controlling the inter-particle distance, the resonance of metal nanoparticles can be tuned. For instance, it was reported that the resonance wavelength of AuNP or silver nanoparticle (AgNP) was readily tuned by self-assembling those 2D arrays and controlling the inter-particle distances using alkylamine.[19]
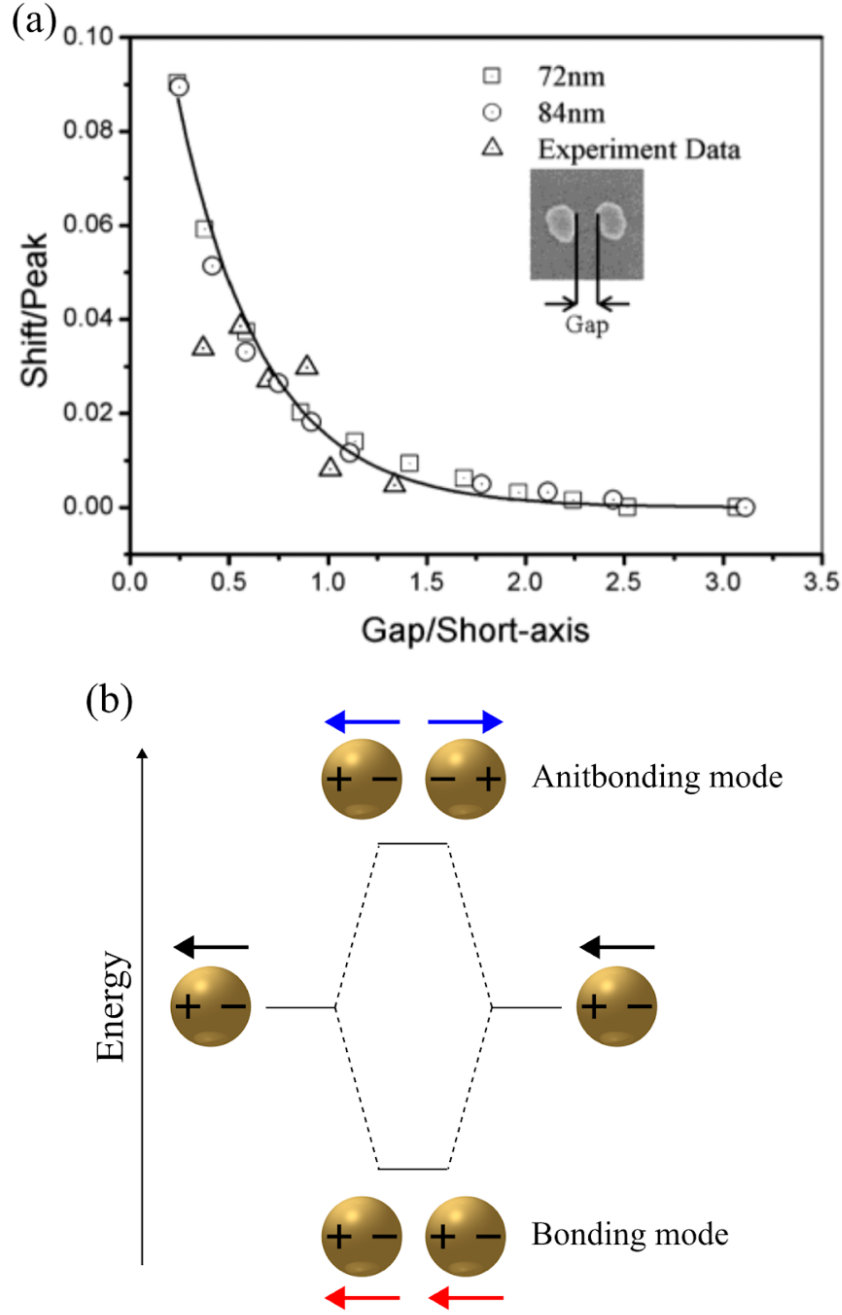
Figure 1-5. (a) Comparison of calculated (□, ○) and experimentally (Δ) measured resonant wavelength shifts as a function of the gap distance between two particles. The resonant shifts and the gaps were scaled by the peak wavelengths and particle short-axis lengths, respectively. (b) Energy diagram to represent typical dipole plasmon and hybridized plasmon by shortening the inter-particle distance.

## 1.2    Surface-enhanced Raman scattering spectroscopy

Metallic nanostructures confine the incident light at the sub-wavelength space and enhance the intensity of light by several orders via the LSPRs. At the metal nanosurface, the localized light shines on the objects more brightly, compared to cases without the metal nanostructures. The effect enhances the signals from target objects such as molecules in spectroscopy. Therefore, the metal nanostructures have been frequently applied to spectroscopy. For instance, application of the structures to fluorescence spectroscopy is called surface plasmon-field enhanced fluorescence spectroscopy, which is available to the interface detection because of higher sensitivity and lower background noise.[20] Those spectroscopic techniques are expected for molecular sensing devices, biosensing, and so on.

One of the most intensely studied spectroscopic applications is surface-enhanced Raman scattering spectroscopy (SERS). Raman scattering spectroscopy is vibrational spectroscopy and gives the information of chemical bonds in molecules and the chemical structures.[21] Although the technique is a promising tool to identify unknown samples, it is commonly employed to study the solid or high concentration solution samples because the signal intensity is much lower than that of other spectroscopic methods such as infrared absorption spectroscopy. In the 1970s, it was reported that the remarkably strong Raman scattering from pyridine adsorbed on silver electrodes was observed.[22-24] It is the birth of SERS spectroscopy. Nowadays, SERS is expected to overcome the drawbacks of conventional Raman scattering spectroscopy (Fig.1-6a). The SERS enables the detection of low concentration solution or gas molecules, even the one molecule.[25,26] Figure 1-6(b) shows the measured SERS spectrum and normal Raman spectrum of *para*-toluenethiol (*p*-TT) ethanol solution. For the SERS measurements, the silver nanoparticle (AgNP) array was prepared by self-assembly of AgNPs.[19] The measurement conditions (concentration of *p*-TT, power of incident laser, and acquisition time) were the same for the fair comparison. In the normal Raman spectrum of *p*-TT, the spectrum seems almost flat and tiny peaks were observed. On the other hand, the peaks were clearly observed in the SERS spectrum. Thus, the Raman scattering was enhanced by using the metallic nanostructures.
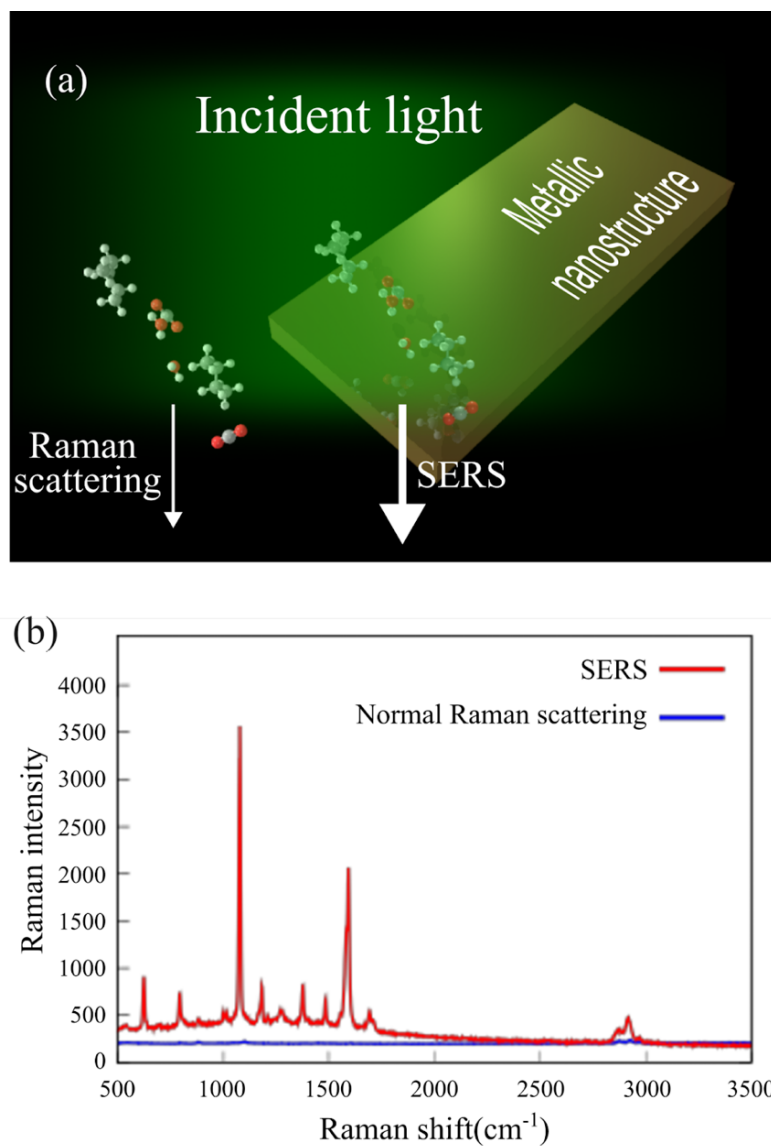
Figure 1-6. (a) Illustration of Raman scattering and SERS from molecules. SERS intensities are much higher than those of Raman scattering because the metallic nanostructure enhances those intensities through LSPR. (b) SERS and normal Raman scattering spectra when the measurements conditions are the same. The target molecule was *p*-TT.

## 1.3　SERS monitoring of plasmon-induced chemical reaction

In the study on SERS spectroscopy, it was revealed that the spectral shape was transformed during the measurements. Our group also observed the transformation of the spectral shape.[27] For the SERS measurements, AgNP two-dimensional (2D) arrays resonating with an excitation wavelength of 532 nm were prepared by employing the self-assembling method and transferring the 2D arrays on the glass substrates, resulting in SERS substrates as shown in Fig.1-7(a). As target molecule, the spectra of $p$-aminothiophenol ($p$-ATP) were measured (Fig.1-7b). It was known that the spectral shape of $p$-ATP was transformed, however the reason was not elucidated. Figure 1-7(c) shows the series of SERS spectra measured as ascending the excitation intensity from 4 to 4000 W/mm$^2$. By comparing the spectral shapes, it was obviously observed that the shape changed at the spectral ranges marked by pink regions. It was found that peaks were newly grown at 1140 cm$^{-1}$, 1390 cm$^{-1}$, and 1430 cm$^{-1}$. On the other hand, the spectra were measured as descending laser intensity from 4000 to 4 W/mm$^2$ as shown in Fig.1-7(d). At the laser intensity of 4000 W/mm$^2$, the newly grown peaks were observed. Interestingly, the peaks were still observed at 4 W/mm$^2$ although the peaks were not observed in the case of measurements with ascending laser intensity. The comparison of the spectral transitions between ascending and descending laser intensities implied that the grown peaks were independent of the laser intensities. From the result, it can be considered that the peaks were derived from the new molecule produced from $p$-ATP. Furthermore, the peaks were assigned to the N=N.[28] Therefore, it was concluded that the $p$-ATP was dimerized to form the N=N during the SERS measurements (Fig.1-7e).

The reaction is currently known as "plasmon-induced chemical reaction". A wide variety of reactions has been reported such as epoxidation, dissociation of hydrogen and reduction of carbon dioxide.[29-31] The reaction was classified into three categories.[32] Firstly, the high energetic electron and hole pairs generated by the energy transfer from light to free electrons drives the scission of chemical bonds of molecules. Secondly, the light excites the electrons in molecules which strongly combine with the metallic surface, and the holes are generated and remain in the metal. Thirdly, the enhanced electric field drives the molecular dissociation. The heat generated through the process of plasmon might also assist the sorts of chemical reactions. The function to assist the chemical

reaction is expected as one of the effective paths to convert the light energy to chemical energy. Therefore, the application of metal nanostructures to new photochemical reaction fields has been enthusiastically studied.
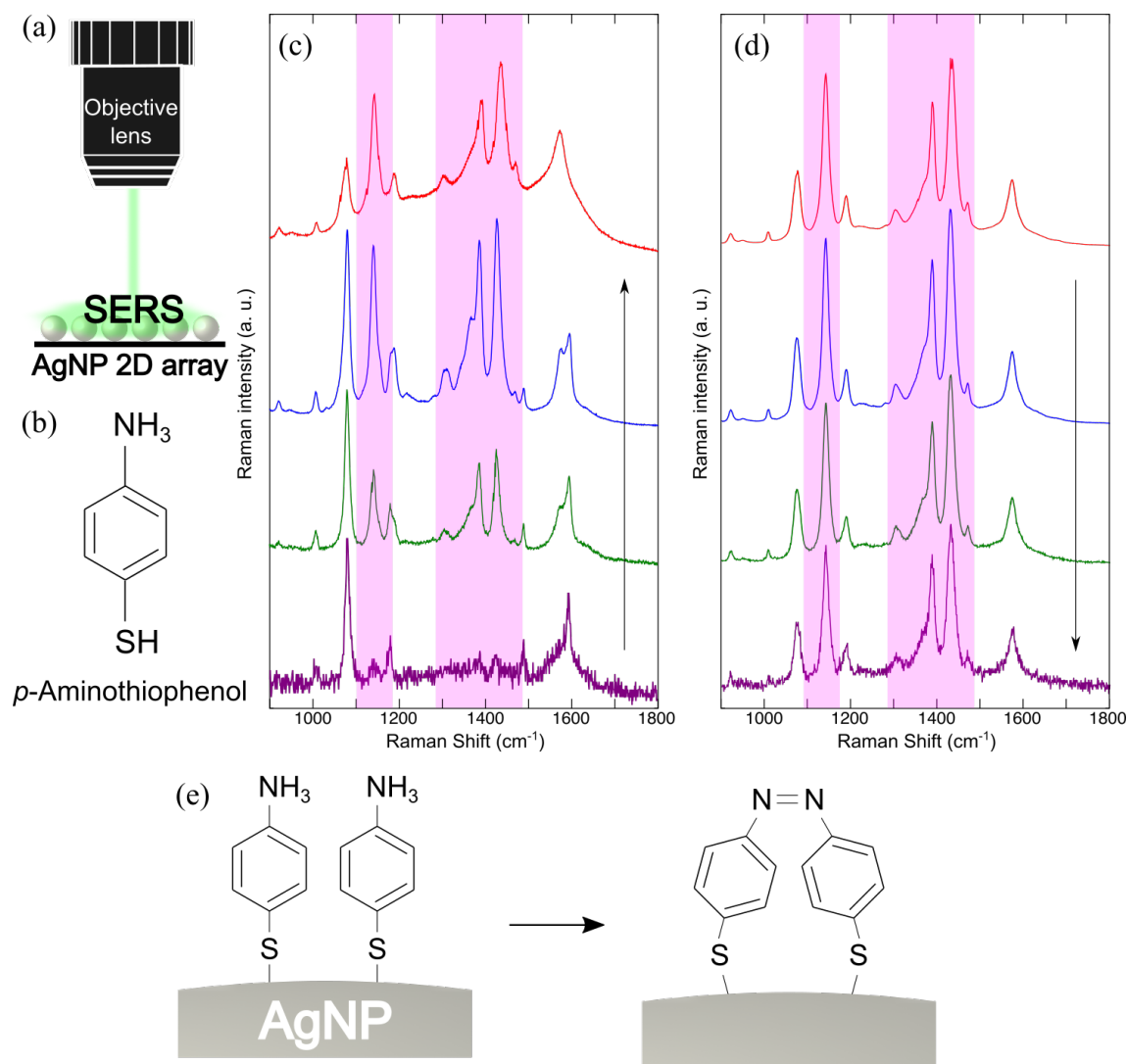


Figure 1-7. (a) A scheme of SERS measurements using AgNP 2D arrays. (b) Chemical structure of *p*-ATP. SERS spectra of *p*-ATP were measured with different excitation laser intensities, 4 (purple), 40 (green), 400 (blue) and 4000 $W/mm^2$ (red). The spectra were measured with (c) ascending and (d) descending the laser intensities. (e) Expected chemical reaction occurred during the measurement.

## 1.4    Reference

1. Jeevanandam, J.; Barhoum, A.; Chan, Y. S.; Dufresne, A.; Danquah, M. K., Review on nanoparticles and nanostructured materials: history, sources, toxicity and regulations. *Beilstein J. Nanotechnol.* **2018**, *9,* 1050–1074.

2. Castro Neto, A. H.; Guinea, F.; Peres, N. M. R.; Novoselov, K. S.; Geim, A. K., The electronic properties of graphene. *Rev. Mod. Phys.* **2009**, *81*, 109.

3. Dresselhaus, M.S.; Dresselhaus, G.; Saito, R., Physics of carbon nanotubes. *Carbon* **1995**, *33*, 883-891.

4. Krenn, J. R.; Weeber, J. C.; Dereux, A.; Bourillot, E.; Goudonnet, J. P.; Schider, B.; Leitner, A.; Aussenegg, F. R.; Girard, C., Direct observation of localized surface plasmon coupling. *Phys. Rev. B* **1999**, *60*, 5029.

5. Kelly, K. L.; Coronado, E.; Zhao, L. L.; Schatz, G. C., The Optical Properties of Metal Nanoparticles: The Influence of Size, Shape, and Dielectric Environment. *J. Phys. Chem. B* **2003**, *107*, 668– 677.

6. Li, D.-B.; Sun, X.-J.; Jia, Y.-P.; Stockman, M. I.; Paudel, H. P.; Song, H.; Jiang, H.; Li, Z.-M., Direct observation of localized surface plasmon field enhancement by Kelvin probe force microscopy. *Light: Science & Applications* **2017**, *6*, e17038.

7. Barnes, W. L.; Dereux, A.; Ebbesen, T. W. Surface plasmon subwavelength optics. *Nature* **2003**, *424*, 824– 830.

8. Murray, W. A.; Barnes, W. L. Plasmonic materials. *Adv. Mater.* **2007**, *19*, 3771−3782.

9. Cinel, N. A.; Butun, S.; Ozbay, E. Electron beam lithography designed silver nano-disks used as label free nano-biosensors based on localized surface plasmon resonance. *Opt. Express* **2012**, *20*, 2587− 2597.

10. Gonzalez-Martinez, I.; Bachmatiuk, A.; Bezugly, V.; Kunstmann, J.; Gemming, T.; Liu, Z.; Cuniberti, G.; Rümmeli, M. Electron-Beam Induced Synthesis of Nanostructures: a Review. *Nanoscale* **2016**, *8*, 11340−11362.

11. Cao, Y. Y.; Takeyasu, N.; Tanaka, T.; Duan, X. M.; Kawata, S. 3D Metallic Nanostructure Fabrication by Surfactant-Assisted Multiphoton-Induced Reduction. *Small* **2009**, *5*, 1144−1148.

12. Nikoobakht, B.; El-Sayed, M. A., Preparation and growth mechanism of gold nanorods (NRs) using seed-mediated growth method, *Chem. Mater.* **2003**, *15*, 1957–

1962.

13. Huang, C.-p.; Yin, X.-g.; Huang, H.; Zhu, Y.-y. Study of Plasmon Resonance in a Gold Nanorod with an LC Circuit Model. *Opt. Express* **2009**, *17*, 6407−6413.

14. Millstone, J. E.; Métraux, G. S.; Mirkin, C. A. Controlling the Edge Length of Gold Nanoprisms via a Seed-Mediated Approach. *Adv. Funct. Mater.* **2006**, *16*, 1209−1214.

15. Park, J.-E.; Lee, Y.; Nam, J.-M. Precisely Shaped, Uniformly Formed Gold Nanocubes with Ultrahigh Reproducibility in Single- Particle Scattering and Surface-Enhanced Raman Scattering. *Nano Lett.* **2018**, *18*, 6475−6482.

16. Fabris, L. Gold Nanostars in Biology and Medicine: Understanding Physicochemical Properties to Broaden Applicability. *J. Phys. Chem. C* **2020**, *124*, 26540−26553.

17. Su, K.-H.; Wei, Q.-H.; Zhang, X.; Mock, J.; Smith, D. R.; Schultz, S. Interparticle coupling effects on plasmon resonances of nanogold particles. *Nano Lett.* **2003**, *3*, 1087−1090.

18. Nordlander, P.; Oubre, C.; Prodan, E.; Li, K.; Stockman, M. I. Plasmon hybridization in nanoparticle dimers. *Nano Lett.* **2004**, *4*, 899−903.

19. Kagawa, R.; Takeyasu, N.; Kaneta, T.; Takemoto, Y. Oil-in-water emulsion as fabrication platform for uniform plasmon-controlled two-dimensional metallic nanoparticle array. *Appl. Phys. Express* **2016**, *9*, 075003.

20. Knoll, W. Interfaces and thin films as seen by bound electromagnetic waves. *Annu. Rev. Phys. Chem.* **1998**, *49*, 569-638.

21. Raman, C. V.; Krishnan, K. S., A New Type of Secondary Radiation. *Nature* **1928**, *121*, 501-502.

22. Fleischmann, M.; Hendra, P. J.; McQuillan, A. J. Raman Spectra of Pyridine Adsorbed at a Silver Electrode. *Chem. Phys. Lett.* **1974**, *26*, 163−166.

23. Albrecht, M. G.; Creighton, J. A. Anomalously Intense Raman Spectra of Pyridine at a Silver Electrode. *J. Am. Chem. Soc.* **1977**, *99*, 5215−5217.

24. Jeanmaire, D. L.; Van Duyne, R. P. Surface Raman Spectroelectrochemistry: Part I. Heterocyclic, Aromatic, and Aliphatic Amines Adsorbed on the Anodized Silver Electrode. *Journal of Electroanalytical Chemistry and Interfacial Electrochemistry* **1977**, *84*, 1−20.

25. Nie, S.; Emory, S. R., Probing Single Molecules and Single Nanoparticles by Surface-Enhanced Raman Scattering, *Science* **1997**, *275*, 1102-1106.

26. Kneipp, K.; Wang, Y.; Kneipp, H.; Perelman, L. T.; Itzkan, I.; Dasari, R. R.; Feld, M. S., Single Molecule Detection Using Surface-Enhanced Raman Scattering (SERS), *Phys. Rev. Lett.* **1997**, *78*, 1667.

27. Takeyasu, N.; Kagawa, R.; Sakata, K.; Kaneta, T. Laser Power Threshold of Chemical Transformation on Highly Uniform Plasmonic and Catalytic Nanosurface. *J. Phys. Chem. C* **2016**, *120*, 12163−12169.

28. Huang, Y.-F.; Zhu, H.-P.; Liu, G. K.; Wu, D.-Y.; Ren, B.; Tian, Z.-Q. When the Signal is Not from The Original Molecule To Be Detected: Chemical Transformation of *para*-Aminothiophenol on Ag during The SERS. *J. Am. Chem. Soc.* **2010**, *132*, 9244−9246.

29. Christopher, P.; Xin, H.; Linic, S. Visible-Light-Enhanced Catalytic Oxidation Reactions on Plasmonic Silver Nanostructures. *Nat. Chem.* **2011**, *3*, 467– 472.

30. Mukherjee, S.; Libisch, F.; Large, N.; Neumann, O.; Brown, L. V.; Cheng, J.; Lassiter, J. B.; Carter, E. A.; Nordlander, P.; Halas, N. J. Hot electrons do the impossible: Plasmon-induced dissociation of $H_2$ on Au. *Nano Lett.* **2013**, *13*, 240−247.

31. Zhang, X.; Li, X.; Zhang, D.; Su, N. Q.; Yang, W.; Everitt, H. O.; Liu, J. Product Selectivity in Plasmonic Photocatalysis for Carbon Dioxide Hydrogenation. *Nat. Commun*. **2017**, *8*, 14542.

32. Kazuma, E.; Jung, J.; Ueba, H.; Trenary, M.; Kim, Y. Real-Space and Real-Time Observation of a Plasmon-Induced Chemical Reaction of a Single Molecule. *Science* **2018**, *360*, 521−526.

# Chapter 2
# SERS monitoring of plasmon-induced chemical reactions

## 2.1 Introduction

When metal nanostructures such as silver nanoparticle (AgNP) and gold nanoparticle (AuNP) are illuminated by light, the incident light is localized at the metal nanosurface via the localized surface plasmons (LSPRs).[1,2] It is well known that the intensity of localized light is a few ten times higher than that of incident light, therefore the metal nanostructures have been applied to spectroscopy. One of the most focused spectroscopic applications is surface-enhanced Raman scattering (SERS) spectroscopy, which is a signal enhancement technique of Raman scattering. The Raman scattering spectroscopy is a kind of vibrational spectroscopy and provides the information about the chemical bonds and the molecular structure. However, it is difficult to detect the target molecule in the solution or the gas molecule since the signal intensity is relatively low, compared to other spectroscopy techniques. SERS spectroscopy which is able to detect even one molecule has been expected to overcome the drawback of Raman scattering spectroscopy.[3,4]

During the research about the application of metallic nanostructures to SERS, it has been revealed that the molecules adsorbed on the metal nanosurface were chemically transformed in the measurements. Our group also confirmed the chemical reaction of *para*-aminothiophenol (*p*-ATP) to *p,p'*-dimercaptoazobenzene (DMAB) by comparing the spectral shape with different incident intensity.[5] The reaction is currently known as plasmon-induced chemical reaction. In more recent years, metallic nanostructures have been applied to photochemical reaction fields. However, there are unclears in plasmon-induced chemical reactions and the application to reaction fields are not progressed.

In this chapter, I evaluated the reactivity of plasmonic structures using AgNP two-dimensional (2D) arrays and 532 nm of excitation wavelength, which excites the LSPR of the arrays. The incident light dependence of plasmon-induced reactions was also investigated from the comparison of the total exposures required for the dimerization at the surface of AgNPs in the different cases of excitation wavelengths and intensities.

Finally, the material dependence of the reaction was further investigated by comparing the reactivity between Ag and Au.

## 2.2 Experiment

### 2.2.1 Materials and Equipment

Silver nitrate (AgNO$_3$, 1st grade, 99.5%), trisodium citrate dihydrate (guaranteed reagent, 99.0%) and sodium tetrahydroborate (practical grade, 90.0%) were purchased from Wako for preparation of AgNP aqueous solutions. Decylamine (1st grade, 98.0%) and stearylamine (1st grade, 98.0%) were purchased from Wako. and n-Hexane (1st grade, 97.0%) was purchased from nacalai tesque for preparation of metal nanoparticle 2D arrays. In this study, the chemical reactions of *p*-ATP (1st grade, 97.0%, Wako), *p*-toluenethiol (*p*-TT, 1st grade, 97.0%, Tokyo Chemical Industry) and 1-buthanthiol (1-BT 1st grade, 97.0%, Tokyo Chemical Industry) were monitored by SERS measurements. SERS measurements were performed using four kinds of excitations (458, 532, 671, and 785 nm). For 532 nm, 671 nm, and 785 nm excitations, the spectra were measured with Raman microscopes (NRS-5100, JASCO; Raman-11, Nanophoton). For 458 nm excitation, we used a home-built micro-Raman spectrometer. Briefly, the beam emitting from argon ion laser was expanded and collimated to fill the pupil of an objective lens. Raman scattering from the sample was collected with the objective lens and was guided to a Czerny-Turner spectrometer (SP- 2500, Acton), equipped with an entrance slit, a blazed grating, and a cooled charge-coupled device (CCD) camera (ProEM 16004, Princeton Instruments).

### 2.2.2 Preparation of metal nanoparticles 2D array for SERS substrate

In order to monitor the plasmon induced chemical reactions of several kinds of molecules, the SERS substrates were prepared using AgNPs or AuNPs. A silver seed solution was prepared by mixing 37.5 mL of water, 0.85 mL of AgNO$_3$ aqueous solution (1.0 w/v%), 10.0 mL of trisodium citrate aqueous solution (1.0 w/v%) and 1.0 mL of NaBH$_4$ aqueous solution (0.1 w/v%), and the mixed solution was kept at 70 °C for an hour. The Ag seed solution (5.0 mL) was mixed with 37.5 mL of water and 1.0 mL of trisodium citrate aqueous solution (1.0 w/v%) and heated to boiling point. Furthermore, 0.85 mL of AgNO$_3$ aqueous solution (1.0 w/v%) was added and heated for an hour. After heating, 1.0 mL of trisodium citrate aqueous solution (1.0 w/v%) and 0.85 mL of AgNO$_3$ aqueous solution (1.0 w/v%) were added and heated for an hour again, resulting in AgNP

aqueous solution. AuNP aqueous solution was prepared by mixing 100 ml of water, 0.5 ml of sodium tetrachloroaurate (III) (0.059M), and 3.5 ml of tri- sodium citrate aqueous solution (3.0 w/v%), and the mixed solution was kept at 80 °C for 3 h.

The resonance wavelengths of Ag and AuNP 2D arrays were tuned to each excitation wavelength without changing the size of the nanoparticles, as reported elsewhere.[6] The array was used for SERS measurements. The AgNP solution was mixed with oil-in-water emulsion prepared with water, n-hexane, and decylamine. Instead of decylamine, stearylamine was used for 2D AgNP and AuNP arrays resonating the excitation wavelengths of 458 nm and 671 nm, respectively. All metal nanoparticle 2D arrays were self-assembled at the interface between n-hexane and water, and those were transferred onto a glass substrate, resulting in SERS active substrates.

### 2.2.3   SERS measurements

Plasmon-induced chemical reactions of *p*-TT, 1-BT, and *p*-ATP were monitored by SERS measurements of those molecules using prepared SERS substrates. For the measurements of *p*-TT, *p*-TT ethanol solution (1 mM) was sandwiched between a cover slip and the AgNP array substrates with a silicone rubber spacer. 1-BT ethanol solution (1 mM) was dropped onto the AgNP array. After the ethanol was dried, the SERS spectra of 1-BT were measured.  The SERS spectra of *p*-ATP were measured after the *p*-ATP ethanol solution (1 mM) was dropped onto the SERS substrates and dried the ethanol.

## 2.3 Results and Discussion

### 2.3.1 SERS measurements of *p*-TT and 1-BT

Firstly, the reactivity of AgNP was investigated by SERS monitoring of the chemical reactions. Figure 2-1(a) shows the SEM image of the AgNP 2D array. The array was transferred on the glass substrate, and it was used for SERS substrates in this experiment. Figure 2-1(b) represents extinction spectrum of the substrate. In the spectrum, two peaks were observed at ~ 400 nm and ~ 550 nm, implying that the substrate resonates with excitation wavelength (532 nm).
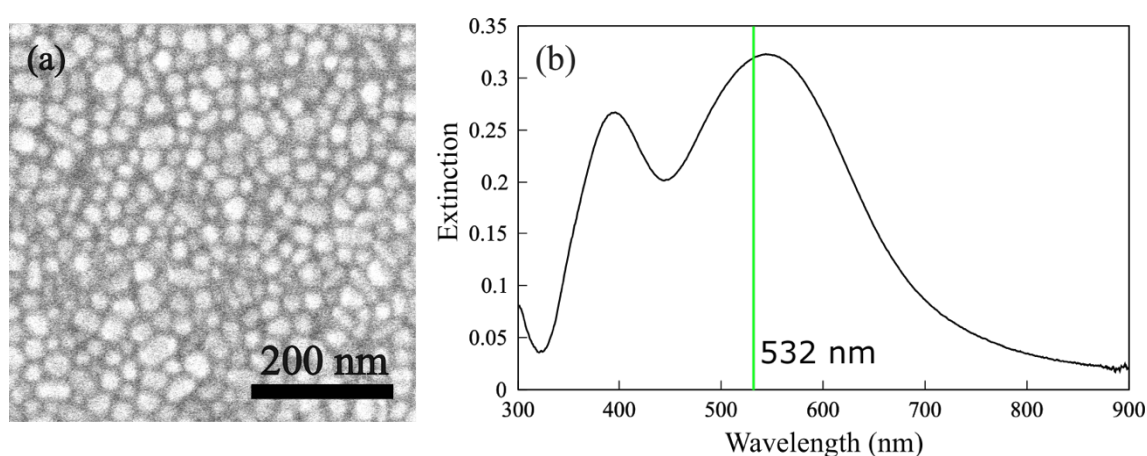


Figure 2-1. (a) The SEM image of the AgNP 2D array prepared by self-assembling AgNPs. (b) Extinction spectra of the SERS substrate.

SERS measurements of *p*-TT ethanol solution (1 mM) were performed using the SERS substrates at the 532 nm excitation by varying incident laser intensity as shown in Fig.2-2(a). At the laser intensity of 4 W/mm$^2$, two distinct peaks were observed at 1080 cm$^{-1}$ and 1600 cm$^{-1}$. Those peaks derived from C-S and methyl groups in the *p*-TT. After the measurements of the *p*-TT at the 400 W/mm$^2$, a shoulder was formed at the ~ 1600 cm$^{-1}$ and a tiny peak was newly observed at 1690 cm$^{-1}$ as indicated by a pink region. The shoulder indicates that substitutes (methyl group) in the aromatic compounds were chemically transformed. Furthermore, the newly appeared peak at 1690 cm$^{-1}$ implies that C=O was formed since the signals from carbonyl groups typically observed at the Raman shift. Therefore, it can be considered that the methyl group in *p*-TT was oxidized to carbonyl group during the measurements at 400 W/mm$^2$ (Fig.2-2b).
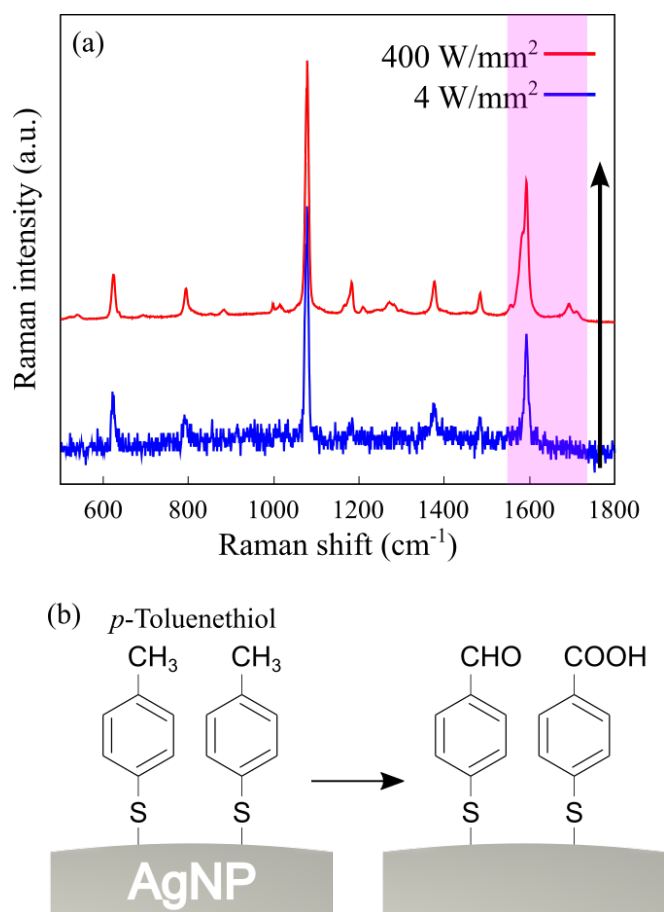
Figure 2-2. (a) SERS spectra of *p*-TT ethanol solution measured at the same position. The excitation laser intensity was increased from 4 (blue) to 400 W/mm$^2$ (red). (b) Structural formula of *p*-TT and schematic illustration of the oxidation at the surface of AgNP.

SERS spectra of 1-BT was also measured using AgNP 2D arrays under excitation of 532 nm by ascending the laser intensities from 4 to 400 W/mm$^2$ as exhibited in Fig. 2-3(a). At 40 W/mm$^2$, several peaks were grown at 1080 cm$^{-1}$, 1580 cm$^{-1}$, and 3050 cm$^{-1}$. The peaks at ~3000 cm$^{-1}$ indicate C-H in 1-BT and, especially the peak newly appeared at 3050 cm$^{-1}$ can be assigned to C-H at C=C. Taking the formation of C=C into account, the two distinct grown peaks at 1080 cm$^{-1}$ and 1580 cm$^{-1}$ might be assigned to the C=C or other chemical bonds at C=C, which corresponds to the fact that Raman signals from the unsaturated carbons are stronger than the that of saturated carbons. From the product, it can be considered that the formation of C=C was caused by dehydrogenation of 1-BT. Those grown peaks became clearer at the laser intensity of 400 W/mm$^2$.

Other Raman peaks were clearly observed at 2870, 2918 and 2960 cm$^{-1}$, which were derived from C-H. Among these Raman peaks, the Raman shift of 2960 cm$^{-1}$ represents C-H in CH$_3$. Interestingly, the changes of peaks derived from C-H at around 3000 cm$^{-1}$ are small although the formation of C$=$C bonds in the molecules, indicating the dehydrogenation preferentially occurs at the secondary carbons (Fig.2-3b). It implies that the radical reactions were dominant at our measurements. Therefore, the oxidation of *p*-TT and 1-BT might be promoted by active oxygens which were radical species generated from oxygen adsorbed on the AgNPs during the excitation of LSPRs.[7]
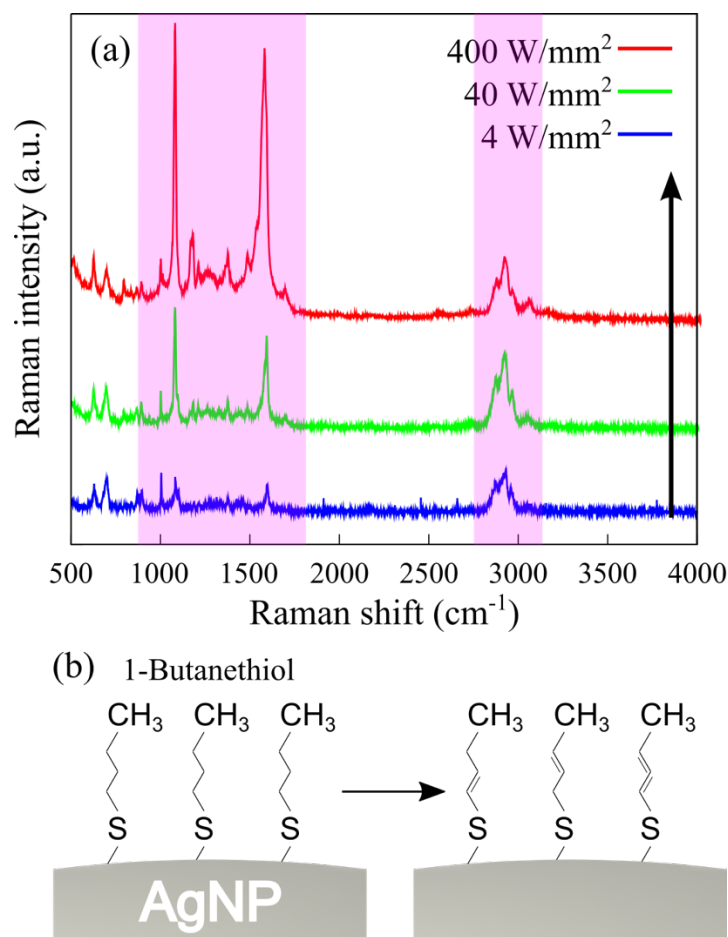


Figure 2-3. (a) SERS spectra of 1-BT measured at the same position. The spectra were measured at laser intensities of 4 (blue), 40 (green), and 400 W/mm$^2$ (red). (b) Structural formula of 1-BT and schematic illustration of the dehydrogenation at the surface of AgNP.

### 2.3.2   Incident light dependence of plasmon-induced chemical reaction

We also investigated the incident light dependence of plasmon-induced chemical reactions. In the study, four excitation wavelengths (458, 532, 671, and 785 nm) were employed.   For the SERS measurements at each excitation, four SERS substrates were prepared from self-assembled AgNP 2D arrays which resonated with each excitation wavelength. Figure 2-4 shows the extinction spectra of each SERS substrate. In the figure, dashed lines represent the excitation wavelengths. The colors of dashed lines and spectra indicate the set of excitation wavelengths and substrates for the SERS measurements. From the comparison of each extinction peak and excitation wavelength, it was confirmed that the SERS substrates resonated with the excitation wavelengths, indicating that all SERS measurements were under on-resonant conditions.
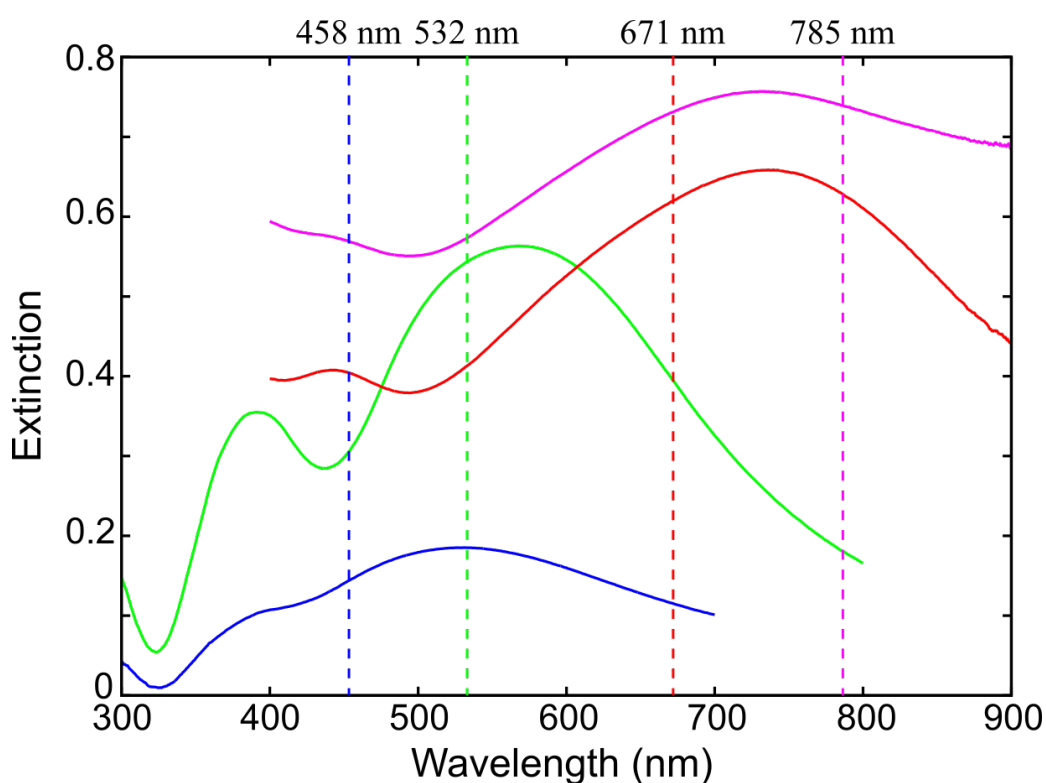


Figure 2-4. Extinction spectra of SERS substrate prepared by self-assembled AgNP 2D arrays. Excitation wavelengths were represented as dashed lines.

The incident light dependence of the plasmon-induced chemical reaction was investigated by SERS monitoring of the dimerization of *p*-ATP to DMAB. For the investigation, it was confirmed that the chemical reaction was induced with all excitations. Figure 2-5 shows the SERS spectra of *p*-ATP measured using each excitation wavelength and SERS substrate with different laser intensities. In the spectra at the excitation wavelength of 785 nm and intensity of 0.033 kW/mm$^2$, three peaks were observed at 1000 cm$^{-1}$, 1080 cm$^{-1}$, and ~1600 cm$^{-1}$ as shown in Fig.2-5(a). When the intensity of the laser increased to 0.33 kW/mm$^2$, the new peaks appeared at 1140 cm$^{-1}$, 1390 cm$^{-1}$, and 1430 cm$^{-1}$, which were assigned to N=N in the molecules.[8] The newly grown peaks became clearer at 3.3 kW/mm$^2$. For other excitation wavelengths, peaks derived from N=N were also observed although laser intensities and relative height of the peaks were totally different. From the spectra, it was concluded that *p*-ATP was dimerized to DMAB for all excitation wavelengths.
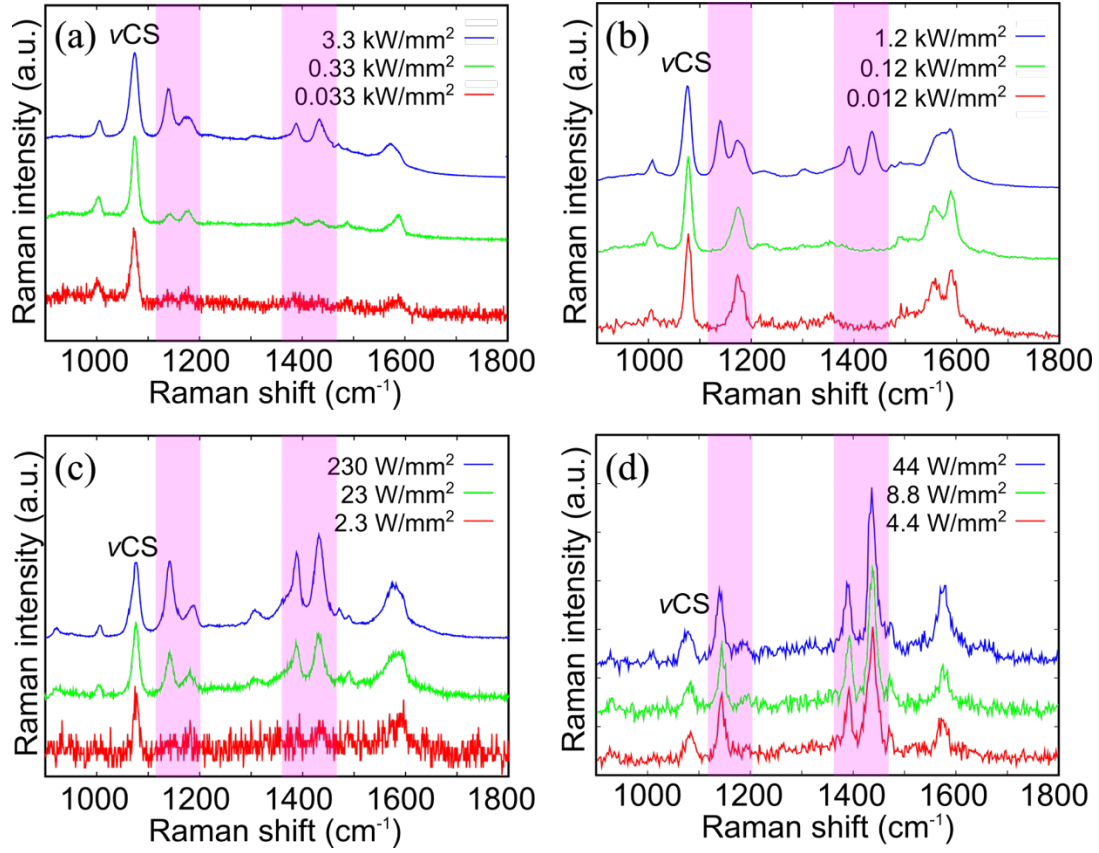
Figure 2-5. SERS spectra of *p*-ATP at the excitation wavelength of (a) 785, (b) 671, (c) 532, and (d) 458 nm.

For the evaluation of the incident light dependence, I focused on the two peaks at 1080 cm$^{-1}$ and 1140 cm$^{-1}$. Generally, the intensity of Raman scattering is linearly proportional to the number of molecules in the illumination spot and the intensity of incident light as following,

$$I_{Raman} \propto N_{molecule}I_{incident}$$

Because the peak at 1080 cm$^{-1}$ is derived from C-S and it is intrinsic chemical bond in both *p*-ATP and DMAB, the intensity is dependent on the total number of those molecules.

$$I_{1080} \propto N_{p\text{-}ATP+DMAB}I_{incident}$$

On the other hand, the peak at 1140 cm$^{-1}$ is derived from the DMAB, therefore the peak intensity is proportional to the number of the DMAB.

$$I_{1140} \propto N_{DMAB}I_{incident}$$

31

From the ratio of those peak intensities, the yields of DMAB in the total molecules can be estimated as follows.

$$I_{1140}/I_{1080} \propto N_{DMAB}I_{incident}/N_{p\text{-}ATP+DMAB}I_{incident} = N_{DMAB}/N_{p\text{-}ATP+DMAB}$$

Figure 2-6 shows the plot of the intensity ratio according to the total exposure which was calculated from the multiplication of the laser intensity and the total exposure time for each measurement of the SERS spectrum. Because the ratio reflects the yield of DMAB, the plot indicates the required amount of exposure to obtain the certain yields of DMAB from $p$-ATP. For the excitation wavelength of 785 nm, the value of ratio increased as increasing the total exposure, meaning that the chemically transformation of $p$-ATP to DMAB proceeded and the yields of DMAB was increased during the reiteration of the SERS measurements as shown in Fig.2-6(a). At the laser intensity of 1650 W/mm$^2$, the ratio reached to ~ 0.6 at the last SERS measurement. The ratio was comparable with the case of 671 nm at 1160 W/mm$^2$ (Fig.2-6b). However, the required total exposures at 671 nm were ~ 100 times lower than that at 785 nm. The ratio was further increased at the even smaller amount of exposure in the case of 532 nm as shown in Fig.2-6(c). For 458 nm, slope of the plot was not observed, implying that most of the $p$-ATP was dimerized at the first SERS measurement as presented in Fig.2-6(d). Those results prove the shorter excitation wavelength was favorable for the chemical reaction. Apart from the comparison of the reaction among excitation wavelengths, the plot also shows the incident intensity dependence. For 785 nm, it was found that the slope of the plot was steeper when the incident intensity was higher although the total exposure was the same. The tendency was also observed for 671 nm and 532 nm of the excitation. In Fig.2-6(d), the slope was not formed, revealing that the chemical transformation was almost finished at the first measurement using even the lowest incident intensity (4.4 W/mm$^2$). In conclusion, it can be considered that the plasmon-induced chemical reaction might be promoted when the excitation wavelength is shorter, and the incident intensity is higher.[9]
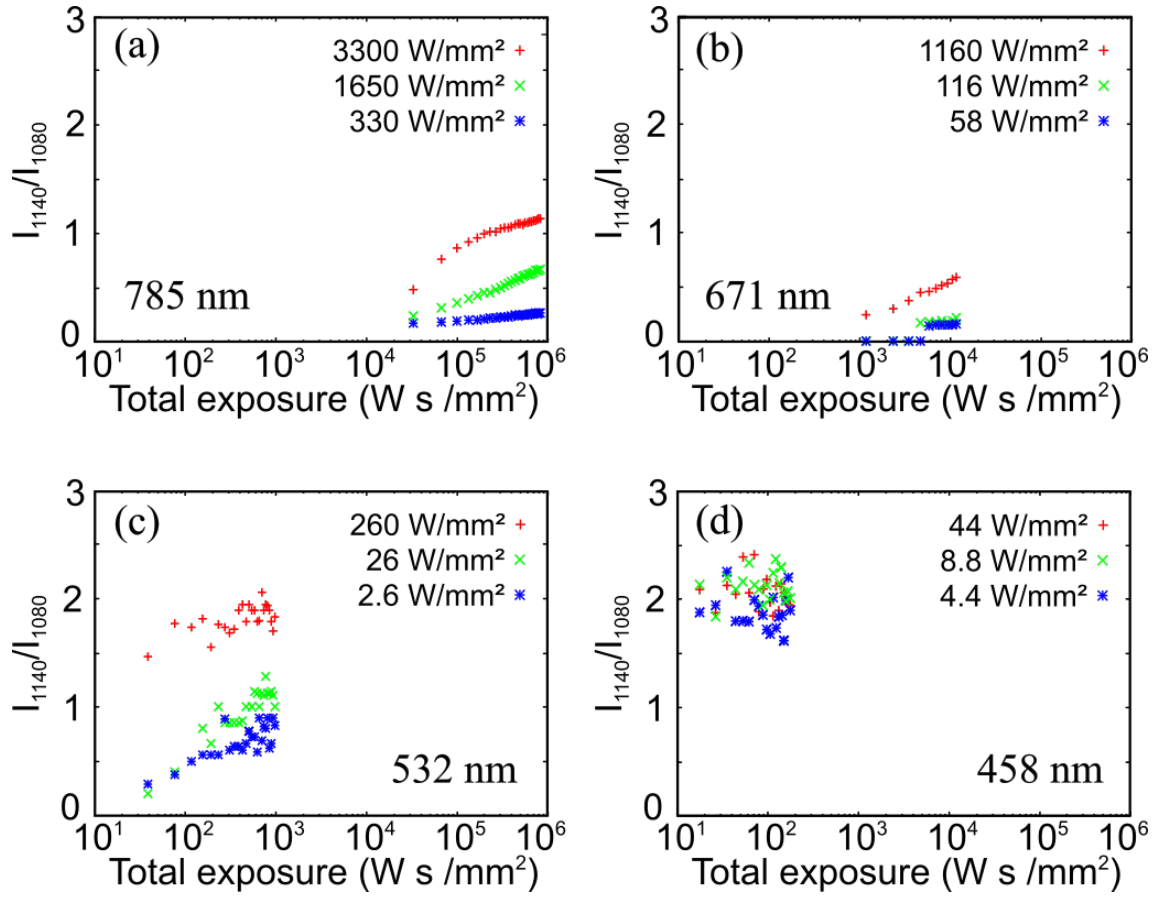
Figure 2-6. Relationship between total exposure and peak intensity at 1140 cm$^{-1}$ at different laser intensities for (a) 785, (b) 671, (c) 532, and (d) 458 nm excitations, where $I_{1140}$ was normalized by $I_{1080}$.

### 2.3.3 Material dependence of plasmon-induced chemical reaction

The material dependence of the reaction was also investigated by comparing the reactivity between Au and Ag, which are representative plasmonic materials. For the evaluation of the dependence, SERS substrates were prepared by self-assembled AuNPs or AgNPs 2D arrays. Those extinction spectra are exhibited as Fig.2-7(a). In this study, those resonance wavelengths were tuned to 671 nm, which was the excitation wavelength to measure the SERS spectra. SERS monitoring of the reaction of $p$-ATP to DMAB was repeated to evaluate the material dependence. Figure 2-7(b) shows the SERS spectrum of $p$-ATP on AuNPs at first and last shots of laser irradiation with the intensity of 57 W/mm$^2$. By comparing the spectra, the newly growth of the peaks were observed at 1140 cm$^{-1}$, 1390 cm$^{-1}$, and 1430 cm$^{-1}$, indicating that the DMAB was produced. The spectral transition was also observed at AgNPs as shown in Fig.2-7(c). Therefore, it was revealed that the $p$-ATP was dimerized to DMAB on both surfaces of Au and Ag during the SERS measurements. From the comparison of SERS spectra at the last measurements between AuNPs and AgNPs, the peak heights were different although the measurement conditions were the same except for the materials.

As well as the study on incident light intensity dependence, the ratio of peak intensities derived from DMAB and C-S was calculated at each measurement and the values were plotted, as shown in Fig.2-7(d) and (e). For AuNPs, it was found that the value of ratio was higher when the laser intensity was higher by comparing the values at the same exposure. For the AgNPs, the value of the ratio was also the highest at 336 W/mm$^2$. On the other hand, the ratios at 116 W/mm$^2$ and 57 W/mm$^2$ were comparable at some points of total exposure (*e.g.*, $10^4$ Ws/mm$^2$). The comparable ratios might be caused by the electric fields formed at the 116 W/mm$^2$ were also equivalent to the case of 57 W/mm$^2$ due to the defects of the AgNP array. Because the measurement conditions were totally same for Au and Ag, the plots can be directly compared and the slope at Ag was found to be steeper than the case of Au, indicating that the chemical reaction of $p$-ATP was more promoted for the AgNPs. Thus, it can be concluded that the plasmon-induced chemical reactions are favorably promoted at the Ag rather than Au.[10]
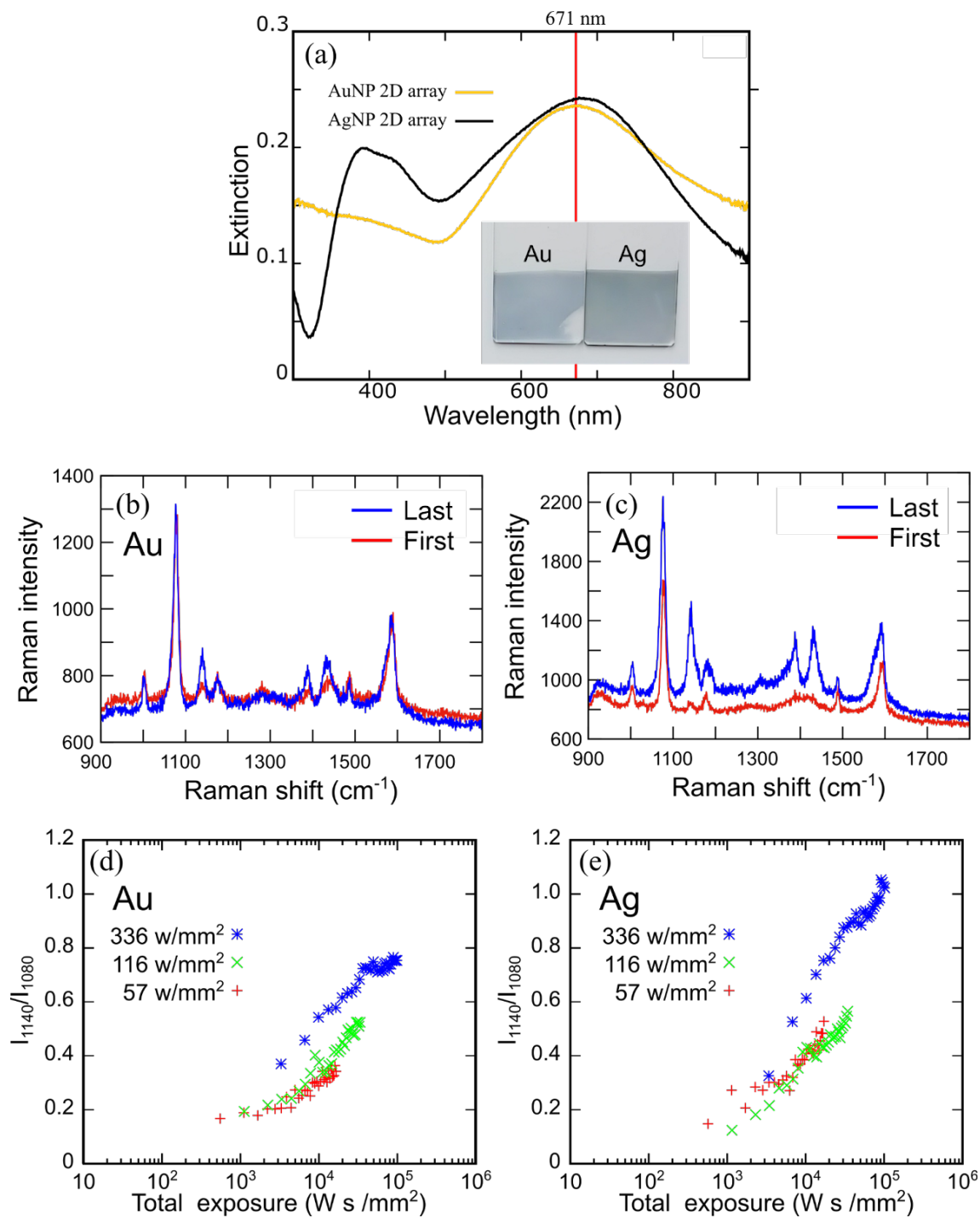
Figure 2-7. (a) Extinction spectra of SERS substrates prepared by self-assembling AuNPs or AgNPs to the 2D arrays. SERS spectra of *p*-ATP measured on (b) AuNP 2D arrays and (c) AgNP 2D arrays. Relationship between total exposure and peak intensity at 1140 cm$^{-1}$ obtained from (d) AuNP 2D arrays and (e) AgNP 2D arrays, where $I_{1140}$ was normalized by $I_{1080}$.

## 2.4 Conclusion

Plasmon-induced chemical reactions were monitored by SERS spectroscopy. For the SERS measurements, AgNPs and AuNPs were self-assembled to the 2D arrays and the arrays were transferred on the glass substrates, resulting in SERS substrates. SERS spectra of p-TT revealed that the methyl group was oxidized to the carbonyl group in ethanol during the measurements at the excitation wavelength of 532 nm. Furthermore, it was found that the carbon chains in 1-BT were dehydrogenated and oxidized to form C=C under the atmospheric condition during the SERS measurements. Those spectra also implied that the oxidations of aromatic compounds and saturated hydrocarbons might be promoted by active oxygens which were generated at the surface of AgNPs during the excitation of LSPRs.

The incident light dependence of the plasmon-induced chemical reaction was evaluated by SERS monitoring of the dimerization of p-ATP to DMAB using a variety of excitation wavelengths (458, 532, 671, and 785 nm). For the SERS measurements, SERS substrates resonating with each excitation wavelength were prepared by self-assembled AgNP 2D arrays. The dependence of the reaction was evaluated by comparing the ratios of the peaks derived from DMAB and C-S at the certain amount of the exposure. The comparison of ratios revealed that the shorter excitation wavelengths and higher incident intensity were favored to induce the chemical reaction in the ranging excitations from 458 nm to 785 nm. The material dependence of the plasmon-induced chemical reaction was also investigated by comparing the reactivity of Au and Ag. As well as the experiments of the incident light dependence, the yields of the DMAB were estimated from the ratio of peak intensities from DMAB and C-S observed on the AuNP 2D array and AgNP 2D array which both arrays resonate with excitation wavelength of 671 nm. It was observed that the ratio at Ag was higher than that at Au. In conclusion, the plasmon induced chemical reaction is more promoted at AgNPs, compared to AuNPs.

## 2.5    Reference

1.  Barnes, W. L.; Dereux, A.; Ebbesen, T. W. Surface Plasmon Subwavelength Optics. *Nature* **2003**, *424*, 824−830.

2.  Maier, S. A.; Atwater, H. A. Plasmonics: Localization and Guiding of Electromagnetic Energy in Metal/Dielectric Structures. *J. Appl. Phys.* **2005**, *98* (1), 011101.

3.  Nie, S.; Emory, S. R., Probing Single Molecules and Single Nanoparticles by Surface-Enhanced Raman Scattering, *Science* **1997**, *275*, 1102-1106.

4.  Kneipp, K.; Wang, Y.; Kneipp, H.; Perelman, L. T.; Itzkan, I.; Dasari, R. R.; Feld, M. S., Single Molecule Detection Using Surface-Enhanced Raman Scattering (SERS), *Phys. Rev. Lett.* **1997**, *78*, 1667.

5.  Takeyasu, N.; Kagawa, R.; Sakata, K.; Kaneta, T. Laser Power Threshold of Chemical Transformation on Highly Uniform Plasmonic and Catalytic Nanosurface. *J. Phys. Chem. C* **2016**, *120*, 12163−12169.

6.  Kagawa, R.; Takeyasu, N.; Kaneta, T.; Takemoto, Y. Oil-in-water emulsion as fabrication platform for uniform plasmon-controlled two-dimensional metallic nanoparticle array. *Appl. Phys. Express* **2016**, *9*, 075003.

7.  Takeuchi, Y.; Fujita, T.; Takeyasu, N. Plasmon-Mediated Chemical Transformation from Alkane to Alkene on a Silver Nanoparticle Array under 532 nm Excitation. *Phys. Chem. Chem. Phys.* **2019**, *21*, 7502−7507.

8.  Huang, Y.-F.; Zhu, H.-P.; Liu, G. K.; Wu, D.-Y.; Ren, B.; Tian, Z.-Q. When the Signal is Not from The Original Molecule To Be Detected: Chemical Transformation of *para*-Aminothiophenol on Ag during The SERS. *J. Am. Chem. Soc.* **2010**, *132*, 9244−9246.

9.  Takeuchi, Y.; Violas, A.; Fujita, T.; Kumamoto, Y.; Modreanu, M.; Tanaka, T.; Fujita, K.; Takeyasu, N. Hot Carrier Generation in Two-Dimensional Silver Nanoparticle Arrays at Different Excitation Wavelengths under On-Resonant Conditions. *J. Phys. Chem. C* **2020**, *124*, 13936−13941.

10. Fujita, T.; Takeuchi, Y.; Yamaguchi, K.; Yano, T.; Tanaka, T.; Takeyasu, N. Comparison of hot carrier generation between self-assembled gold and silver

nanoparticle arrays tailored to the same hybrid plasmon resonance, *J. Appl. Phys.* **2020**, *128*(12), 123104.

# Chapter 3
# Linkages of AuNPs fixed on glass substrate

## 3.1　Introduction

Metal nanostructures confine the incident light at the sub-wavelength scale space via the localized surface plasmon resonance (LSPR), where the electric field intensity of the light is enhanced by several orders. While the metal nanostructures have been applied to the spectroscopy such as surface-enhanced Raman scattering (SERS) spectroscopy, it has been reported that a variety of chemical reactions were induced at the metal nanosurface when the molecule and the metal structure were illuminated by light in more recent years.[1-5] The reaction is currently known as plasmon-induced chemical reaction and the plasmonic nanostructure has been expected as the photochemical reaction fields. We also monitored the chemical reaction using SERS spectroscopy. Among them, I monitored the oxidation of $p$-toluenethiol and 1-butanethiol at the surface of silver nanoparticles (AgNPs) under the light illumination.[6] Furthermore, the incident light or material dependences of the plasmon-induced chemical reaction were investigated based on the SERS spectra of $p$-aminothiophenol.[7,8]

Because the metal nanostructures facilitate the chemical reaction of chemically stable molecules, lots of effort has been made to produce the useful molecules using the metal nanostructures at mild conditions. For instance, the reduction of carbon dioxide to methane which is one kind of energy source has been reported.[9] Plasmon-induced chemical reaction has also been focused to achieve green chemistry. Although graphene oxide is generally produced by using deleterious substances such as sulfuric acid, a direct production method from graphene to graphene oxide with the aid of plasmon was proposed.[10] Thus, it is considered that the not only chemical reaction of organic compounds but also modification of inorganic molecules can be induced at the metal nanosurface under the light illumination.

As the reactant for plasmon-induced chemical reaction, I selected the metal ions. The optical property of the metal nanostructures is determined by the geometries, therefore it can be expected that the resonance wavelength of the metal nanostructure is shifted when the geometry of the structures is transformed due the chemical reaction of metal ions at

the metal nanosurface. By the geometrical transformation because of plasmon induced chemical reaction, the resonance wavelength can be tuned by the light illumination as shown in Fig.3-1. In order to confirm the hypothesis, the linked metal nanostructures were selected as the target structures. In this chapter, the linkages of gold nanoparticles (AuNPs) were performed by the light illumination in the presence of gold ions as presented in Fig.3-2. For the confirmation of the linkages, the AuNPs were directly observed using scanning electron microscopy (SEM).

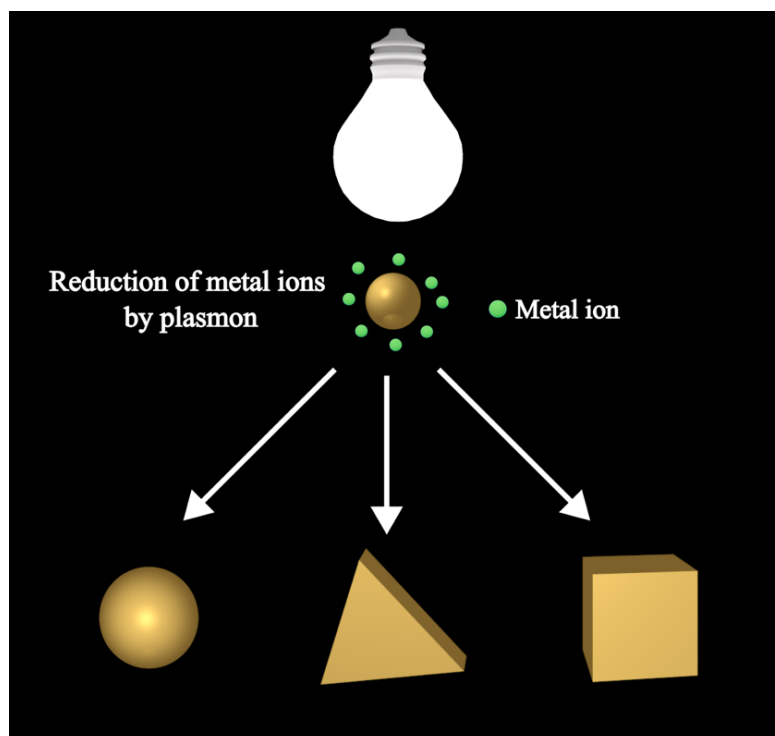Figure 3-1. Concept to modify the geometry of the metal nanoparticle using reductions of metal ions induced by the light localized at metal nanosurface.
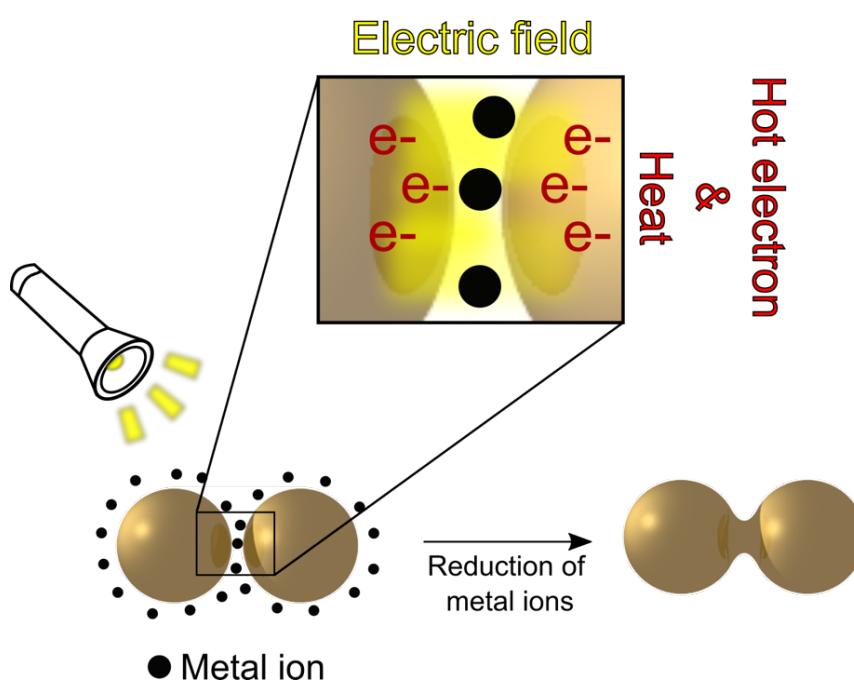


Figure 3-2. Schematic illustration of linkages of metal nanoparticles by plasmon-induced metal ion reductions, where metal ions adjacent to the gap of metal nanoparticles are selectively reduced by enhanced electric field formed by LSPR during light illumination.

## 3.2　Experiment

### 3.2.1　Materials and Equipment

For preparation of AuNPs, gold(III) sodium chloride dihydrate ($NaAuCl_4 \cdot 2H_2O$, guaranteed reagent, 98.0%) and tri-sodium citrate dihydrate (extra pure reagent, 99.0%) were purchased from nacalai tesque. 3-Aminopropyldimethoxymethylsilane (97.0%) obtained from Tokyo Chemical Industry Co., Ltd. and ethanol (99.5%) was purchased from nacalai tesque for direct observation of AuNPs. In order to induce reduction of gold ions, a fluorescent lamp (LOVEEYE, Matsushita Electric Industrial Co., Ltd.) was used. The extinction spectra of those solutions were measured by using a spectrophotometer (UV-3600, SHIMADZU) and generated gold was directly observed by a scanning electron microscope (SEM, SU8010, HITACHI).

### 3.2.2　Photo-induced gold ion reduction with a fluorescent lamp

A $NaAuCl_4$ aqueous solution with the concentration of 20 μM was illuminated with the fluorescent lamp for one day. Before and after light illumination, the extinction spectra of the gold ion solution were measured. The geometry of generated gold was directly observed by SEM.

### 3.2.3　Preparation of AuNPs-fixed substrate

As a plasmonic material, gold nanoparticles (AuNPs) were selected. AuNP aqueous solution was prepared by heating the mixture of $NaAuCl_4$ and sodium citrate in water at 80 °C for 3 hours. By centrifugation of the prepared AuNP aqueous solution with 14000×g for 50 minutes, the 90 % of solvent was replaced with ultrapure water. After repeating the replacement again, the solution was further centrifuged with 14000×g for 50 minutes and the 40% of the solvent was replaced with the ultrapure water, resulting in a washed AuNP aqueous solution.

Amino-coated glass substrate was prepared by the immersion of a hydrophilized glass substrate into the mixture of water, ethanol and 3-aminopropyldimethoxymethylsilane for 1 hour, where the volume ratio between water and ethanol was equivalent. After that, the substrate was washed by water with a sonicator for 40 minutes. The amino-coated glass

substrates were immersed in the washed AuNP aqueous solution for 1 hour, resulting in AuNPs-fixed substrates.

### 3.2.4    Investigation of plasmon-induced gold ion reduction at the gold nanosurface

Reduction of $AuCl_4^-$ (gold ion) at the surface of AuNPs fixed on the substrate was induced by light illumination with the fluorescent lamp for one day, where the AuNPs fixed substrate was immersed into 50 μM of gold ion aqueous solution. The site-selectivity of the reduction was confirmed by comparing the SEM image of the AuNPs fixed on the substrate before and after light illumination as illustrated in Fig. 3-3 (a). The power of the fluorescent lamp was measured at each wavelength ranging from near-ultraviolet to near-infrared regimes using a power meter as shown in Fig. 3-3 (b). In order to investigate the role of gold ions and light illumination, the AuNPs fixed substrate was immersed in water during the light illumination. Also, the AuNPs-fixed substrate was immersed into the gold ion solution, but light was shielded by covering a dish with aluminum foil. SEM images of those AuNPs were also compared before and after light illumination or shielding, respectively.
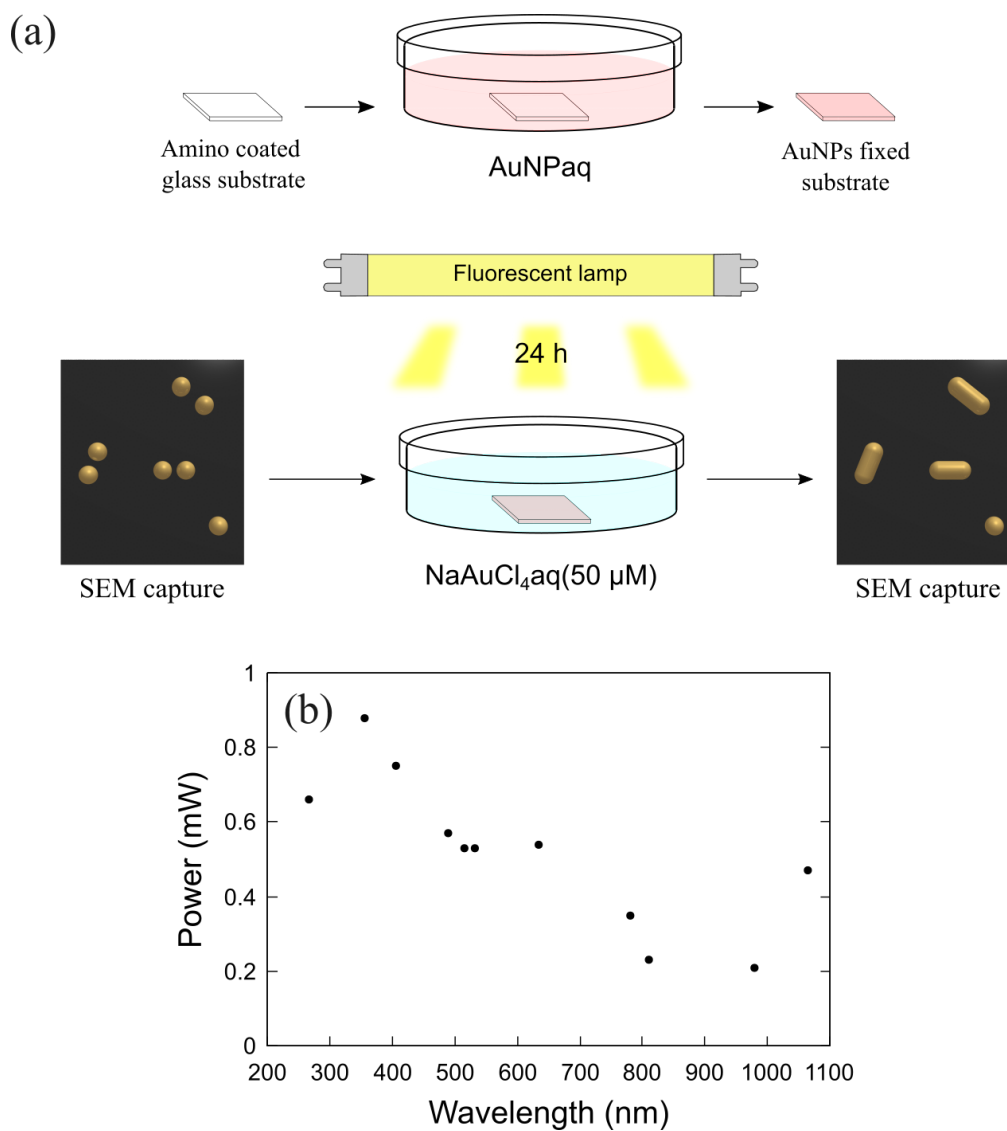
Figure 3-3. (a) Schematic diagram to directly compare the geometry of AuNPs before and after light illumination by using AuNPs-fixed substrates prepared by amino-coated glass substrates. As a light source to induce reduction of gold ions, a fluorescent lamp was used.   (b) Power of the lamp at each wavelength.

### 3.2.5 Simulation of extinction spectra and distribution of electric field intensities

In order to investigate the linkage process of AuNPs, distributions of the electric field intensities were simulated by discrete dipole approximation (DDA).[11] In the approximation, the target object is regarded as an assembly of point dipoles. The optical property of each point dipole was given by Ref.12. The used software was DDSCAT 7.3.3. The electric field was calculated for AuNP dimers and bridged AuNP dimers. The diameter of each nanoparticle was set to 20 nm. For the dimer, the spatial gap between AuNPs was 1 nm. For the bridged AuNPs, the thicknesses of the bridge were 10, 14, 18 nm. The field distribution of each structure was calculated when the structures were illuminated at the wavelength of the LSPR. The resonance wavelength of each structure was also simulated by the DDA calculation.

## 3.3 Results and Discussion

### 3.3.1 Photo-induced gold ion reduction with a fluorescent lamp

The reduction of gold ions by light illumination with the fluorescent lamp was confirmed. Figure 3-4 (a) shows the absorption spectrum of the $NaAuCl_4$ aqueous solution with the concentration of 20 μM and the extinction spectrum of the solution after the light illumination with the fluorescent lamp for one day. In the absorption spectrum of $NaAuCl_4$ aqueous solution before the illumination, a characteristic peak was observed at ~300 nm, indicating the peak derived from gold ions. After the light illumination, the shape of the spectrum was transformed. First, the peak from gold ions decreased and the shape became flat from 300 nm to 500 nm. Alternatively, a new peak was grown at ~550 nm. In order to identify an origin of the peak, SEM observation was performed for the illuminated solution. Figure 3-4 (b) shows the SEM image observed from the illuminated solution after water was dried. Nanoparticles with diameters larger than 50 nm were observed. Because only gold ions existed in the solution, it can be considered that the nanoparticles were composed of gold, in other words, AuNPs. It is generally accepted that the LSPR mode of AuNPs with diameters larger than 50 nm was observed at ~550 nm.[13] The results of the spectrum and the SEM image represent that gold ions were reduced by the light illumination with a fluorescent lamp, resulting in AuNPs.
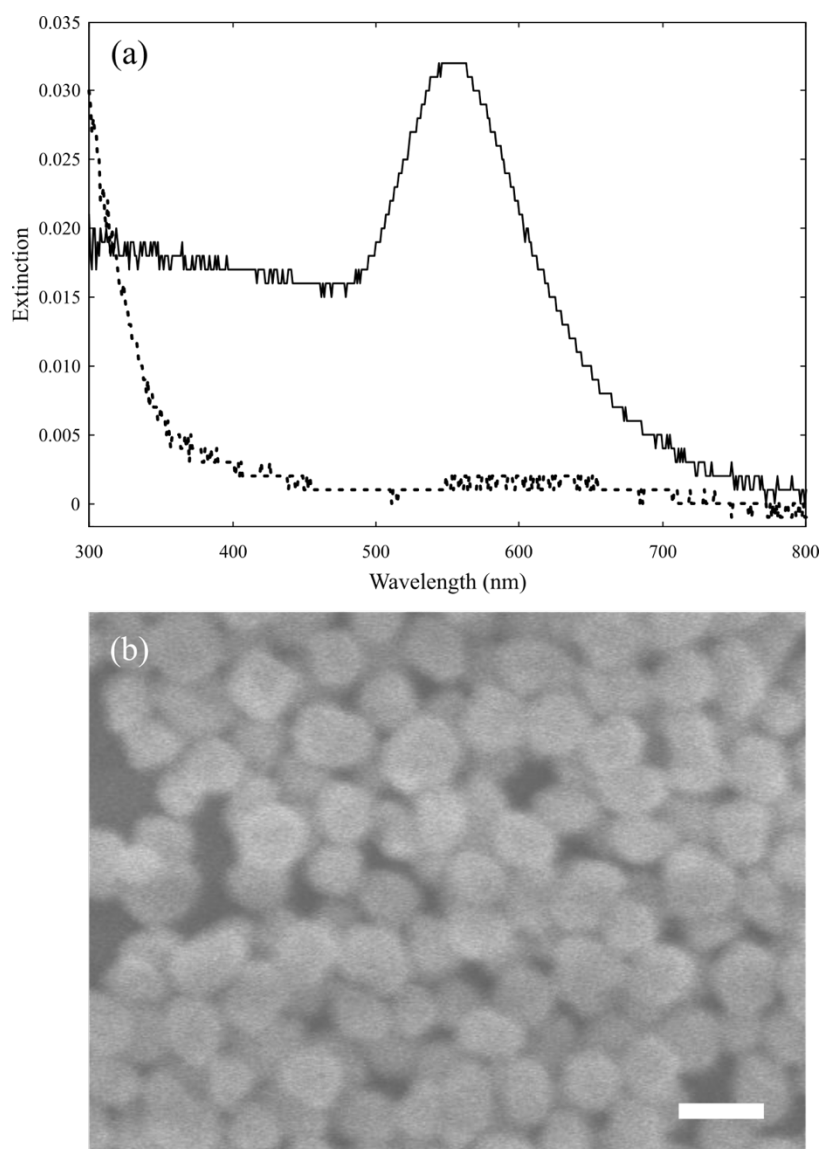
Figure 3-4. (a) Extinction spectra of NaAuCl₄ aqueous solution before (dashed line) and after (solid line) light illumination by fluorescent lamp for one day. The concentration of NaAuCl₄ was 20 μM. (b) SEM image of AuNPs prepared by the illumination of NaAuCl₄ aqueous solution. The scale bar is 100 nm.

### 3.3.2 Preparation of AuNPs-fixed glass substrate

For the monitoring of geometrical transformation of AuNPs, AuNPs were fixed on the glass substrates via the amino group. The amino-coated substrates were prepared by immersion of hydrophilized glass slide into the mixture of 3-aminopropyldimethoxymethylsilane, ethanol and water solution. Each treatment of the substrate was confirmed by the variation of wettability as shown in Fig. 3-5 (a) and (b). The prepared amino-coated glass substrates were soaked in the synthesized AuNP aqueous solution. The red color of the AuNP aqueous solution was transferred to the substrate, indicating AuNPs remained on the substrate as shown in Fig. 3-5 (c). AuNPs fixed on the substrate causes the color transfer because the AuNPs were coated with citric acids and surface charge of AuNPs was negative in the solution due to the deprotonation of citric acid, amino groups which have positive charges bind with citric acid on AuNPs by electrostatic interaction as illustrated in Fig. 3-5 (d).

The SEM image of the fixed AuNPs indicates the nanoparticle monomers with the diameters of 10~15 nm is distributed on the glass substrate with a certain distance between nanoparticles (Fig. 3-5e). The monomers came out the color of substrate, which implies the NPs in SEM images are AuNPs. The AuNPs-fixed substrates were used for comparing the geometry before and after light illumination.
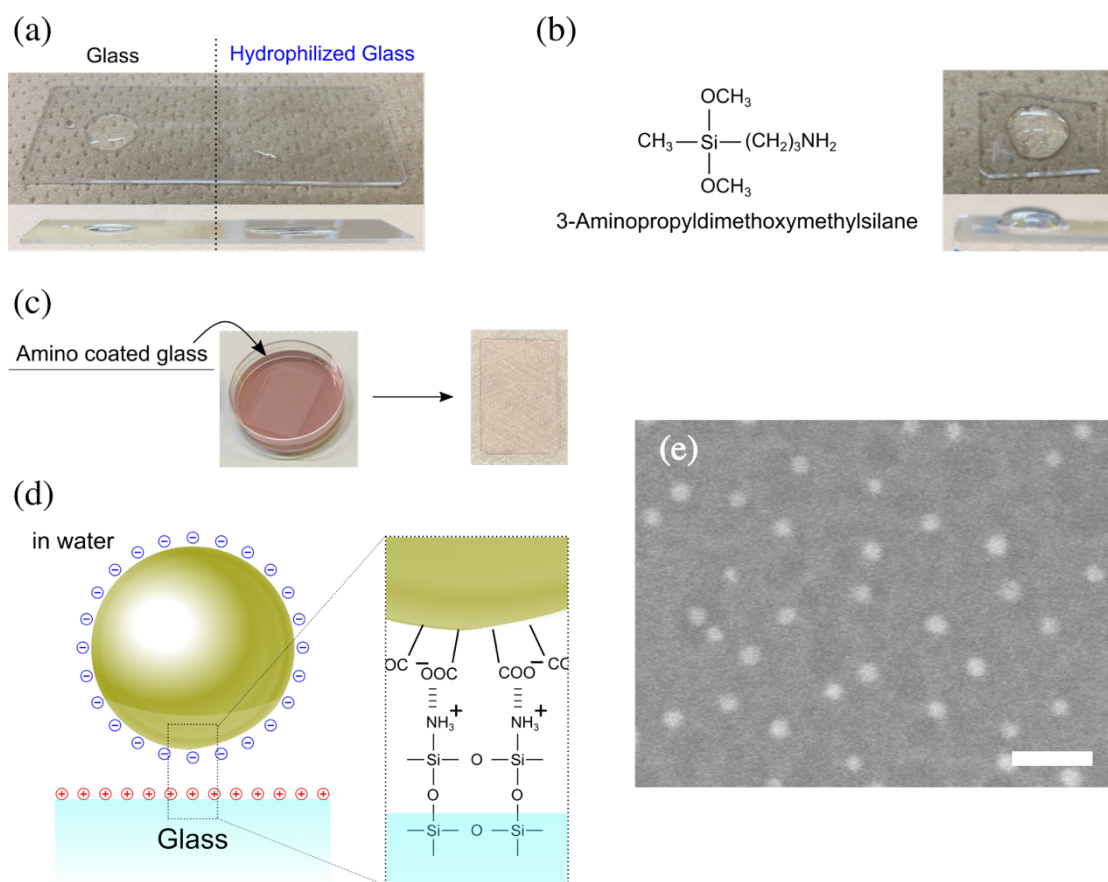
Figure 3-5. Photographs of (a) normal, hydrophilized and (b) amino-coated glass substrates. To visualize the wettability, water was dropped onto each substrate. (c) AuNPs fixed glass substrates and (d) schematic illustration of AuNPs binding with amino coated glass via electrostatic interaction. (e) SEM image of fixed AuNPs on the substrate. The scale bar is 50 nm.

### 3.3.3 Geometrical transformation of fixed AuNPs by light illumination in the presence of gold ions

The AuNPs fixed substrate was immersed into the gold ion aqueous solution (50 μM) and illuminated by the fluorescent lamp. Those SEM images were captured before and after light illumination, displayed in Fig. 3-6 (a) and (b). Because AuNPs were randomly fixed on the substrate, the spot to observe the geometry transformation was selected, where fixed AuNPs were paired. In Figure 3-6 (a), three AuNP pairs were observed and numbered. By the comparison of SEM images before and after light illumination, it was found that the gaps of AuNP pair 1 and 2 were fully filled by the light illumination, resulting in the rod-like structure. Furthermore, the gap of AuNP pair 3 was also partially filled by the illumination in the presence of gold ions. The residual organic molecules including citrate ions adsorbed on the AuNPs were removed by irradiation of ozone after fixing AuNPs on amino-coated glass substrate. The residual gold ions were also washed carefully by water. Therefore, it can be considered that the filling gap might be caused by the reduction of gold ions rather than by precipitation of organic molecules or gold ions.

In order to investigate the roles of gold ions, the AuNP-fixed substrates were immersed in water and illuminated. The SEM images were also observed before and after light illumination as shown in Fig. 3-6 (c,d). The comparison of those images revealed that the geometry of fixed AuNPs were preserved after the light illumination. Furthermore, a light-shielding experiment was also performed. Figure 3-6 (e,f) shows SEM images of fixed AuNPs before and after light-shielding in the presence of gold ions. The gap of the AuNP pair was not filled in the presence of only gold ions. From the results, it can be concluded that both light illumination and gold ions are necessary to promote the gap filling reaction, which implies that gold ion reductions cause the linkages of AuNPs by light illumination.

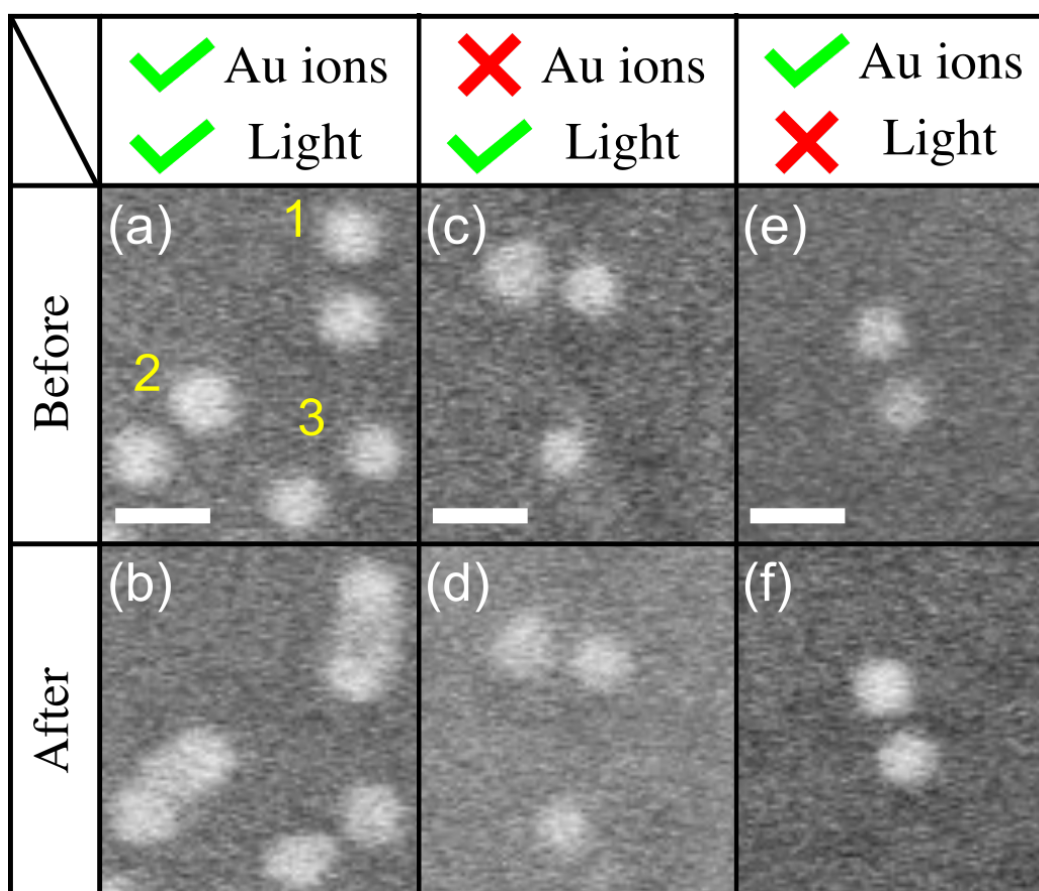| | ✅ Au ions ✅ Light | ❌ Au ions ✅ Light | ✅ Au ions ❌ Light |
|---|---|---|---|
| Before | (a) 1 2 3 | (c) | (e) |
| After | (b) | (d) | (f) |

Figure 3-6. SEM images of AuNPs fixed on glass substrates. Fixed AuNPs in the presence of gold ions (a) before and (b) after light illumination for 24 h. AuNPs were also illuminated without gold ions (c,d) or light-shielded during the immersion of the substrate in the gold ion solution (e,f). The scale bar in all SEM images is 20 nm.

### 3.3.4 Inference of the linkage process by simulated distribution of electric fields

The extinction spectrum and the distribution of the field intensity were simulated by DDA to discuss the linkage process during the light illumination. Figure 3-7 (a) shows the simulated extinction spectrum of a AuNP dimer with 20 nm of diameter, where the gap distance is 1 nm and polarization of incident light is parallel to the long axis of the dimer. The distribution of the electric field intensity was also simulated when the dimer was illuminated at the wavelength of its peak as indicated by a black inverted triangle in the spectrum. The field distribution of the AuNP dimer indicates that the field intensity is strong at the gap between AuNPs, and the intensity is the strongest at the center. The strong field intensity spot is well-known as a "hot spot".

The simulations of the spectrum and the field distributions were also performed for linked AuNP, in other words, Au nanodumbbell (AuND). Figure 3-7 (b) shows the simulation results of AuND with 10 nm of a handle thickness. The peak wavelength is red-shifted to the near-infrared region, compared to the dimer. The field distribution is also modified. For AuND, the hot spots were formed around the handle, especially at the intersection between the AuNPs and the handle.

The simulation results of thicker handle AuNDs are shown in Fig. 3-7 (c,d), where the thicknesses of the handle are 14 nm and 18 nm, respectively. Compared to the 10 nm thickness of the handle, the extinction peak of the AuND with the thickness of 14 nm is blue-shifted. The hot spot is also moved according to the migration of intersections between AuNPs and handles. The localization of the light field is diffused over the surface of the structure, compared to the AuND with 10 nm of handle thickness. The extinction peak is further blue-shifted for AuND with 18 nm of the handle. The localized field is also modified, and the light is localized over the surface of AuND with a thick handle. The series of simulation results indicate that the spot where the light is localized is modified by the linkage of the dimer or by increasing the thickness of the handle.

Figure 3-7 (e) is a schematic illustration of the predicted linkage process of AuNP dimers from the field distribution calculated by the theoretical method. An AuNP dimer is linked at once during the light illumination since the dimer interacts with incident light and confine it into the gap as simulated in Fig. 3-7 (a). After the linkage, the incident light is confined around the handle of AuND. The confined light induces the reduction of gold

ions, and the handle is grown. Finally, the handle of the dumbbell grew to the same diameter of AuNPs at the side of the handle. In Figure 3-6 (a,b), AuNP pairs might support the predicted linkage process. For pair 3, it seems that the growth of AuNPs is site-selectivity occurred at the gap of the pair rather than outer site of the AuNPs. Taking the site-selective reduction of gold ions into account, it is concluded that the growth was promoted accompanying the transition of the electric field distribution formed on the structure.
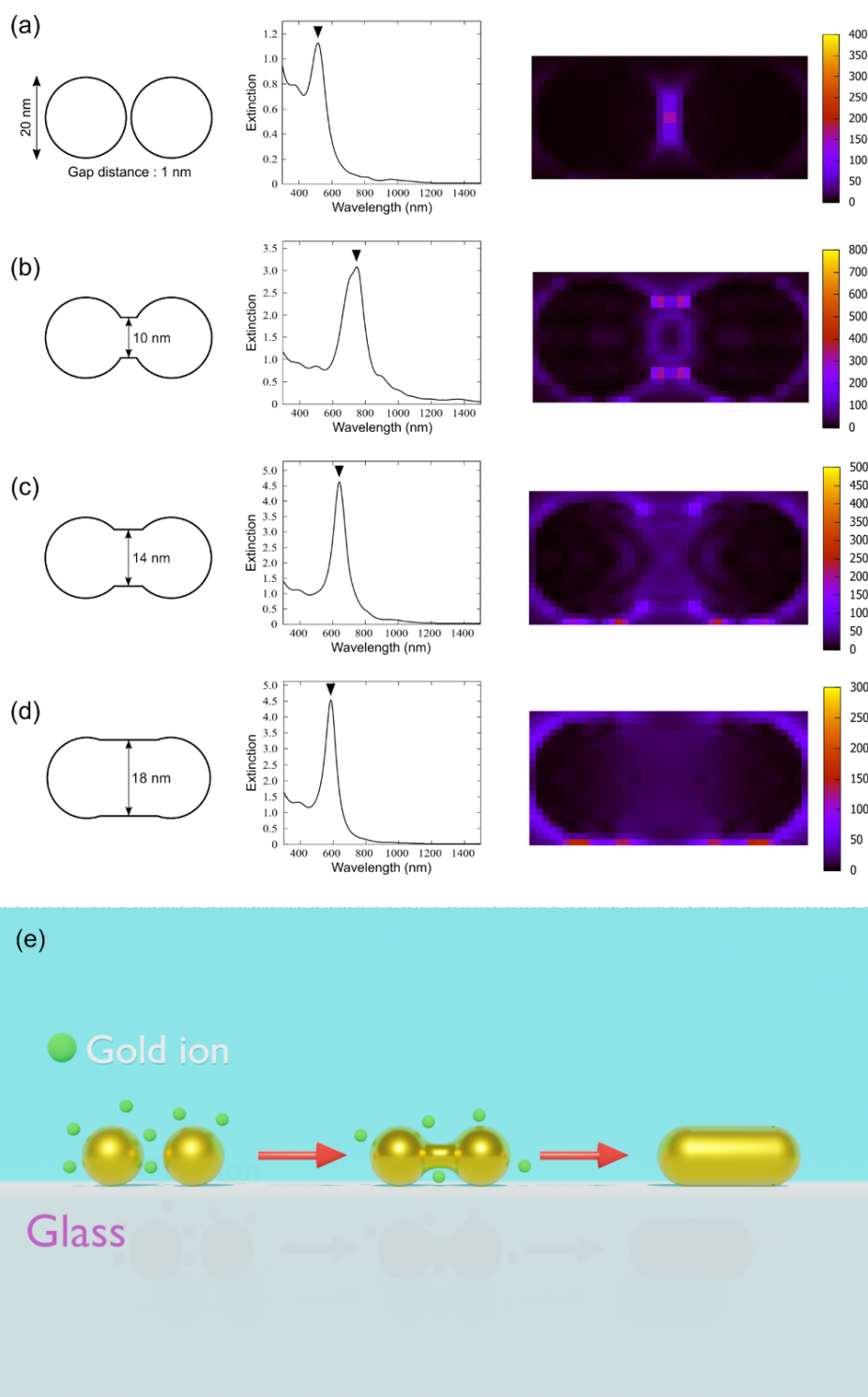
Figure 3-7. Simulation results of extinction spectrum and field intensity distribution for (a) AuNP dimer and (b,c,d) AuNDs with different the handles. The incident wavelength was 530 nm, 780 nm, 620 nm, and 590 nm, respectively. The thickness of the handle was set to (b) 10 nm, (c) 14 nm and (d) 18 nm. (e) Schematic illustration of the linkage and growth process of AuNP dimer in the presence of gold ions during the light illumination.

## 3.4    Conclusion

It was revealed that the gaps of fixed AuNP pairs were filled in the presence of gold ions during the illumination with the fluorescent lamp by the comparison of their SEM images before and after the illumination. Both gold ions and light illumination were necessary to fill the gaps, implying that the AuNPs were linked by the photo-induced gold ions reductions. Furthermore, the linkage process was deduced that the dimer was linked at once, the growth of the handle was promoted accompanying the transition of the electric field distribution on the dimer or the AuNDs by the SEM images and simulation results obtained by DDA. From those results, it can be concluded that the site-selective gold reduction induced by localized light at the metal nanosurface is dependent on the excited LSPR mode.

## 3.5    Reference

1.  Christopher, P.; Xin, H.; Marimuthu, A.; Linic, S.Singular Characteristics and Unique Chemical Bond Activation Mechanisms of Photocatalytic Reactions on Plasmonic Nanostructures. *Nat. Mater.*   **2012**, *11*, 1044– 1050.

2.  Takeyasu, N.; Kagawa, R.; Sakata, K.; Kaneta, T. Laser Power Threshold of Chemical Transformation on Highly Uniform Plasmonic and Catalytic Nanosurface. *J. Phys. Chem. C* **2016**, *120*, 12163−12169.

3.  Bao, J. L.; Carter, E. A. Surface-Plasmon-Induced Ammonia Decomposition on Copper: Excited-State Reaction Pathways Revealed by Embedded Correlated Wavefunction Theory. *ACS Nano* **2019**, *13*, 9944−9957.

4.  Li, S.; Miao, P.; Zhang, Y.; Wu, J.; Zhang, B.; Du, Y.; Han, X.; Sun, J.; Xu, P. Recent Advances in Plasmonic Nanostructures for Enhanced Photocatalysis and Electrocatalysis. *Adv. Mater.* **2021**, *33*, 2000086.

5.  Liang, C.; Lu, Z. A.; Wu, J.; Chen, M. X.; Zhang, Y. Y.; Zhang, B.; Gao, G. L.; Li, S. W.; Xu, P. Recent advances in plasmon- promoted organic transformations using silver-based catalysts. *ACS Appl. Mater. Interfaces* **2020**, *12*, 54266−54284.

6.  Takeuchi, Y.; Fujita, T.; Takeyasu, N. Plasmon-Mediated Chemical Transformation from Alkane to Alkene on a Silver Nanoparticle Array under 532 nm Excitation. *Phys. Chem. Chem. Phys.* **2019**, *21*, 7502−7507.

7.  Takeuchi, Y.; Violas, A.; Fujita, T.; Kumamoto, Y.; Modreanu, M.; Tanaka, T.; Fujita, K.; Takeyasu, N. Hot Carrier Generation in Two-Dimensional Silver Nanoparticle Arrays at Different Excitation Wavelengths under On-Resonant Conditions. *J. Phys. Chem. C* **2020**, *124*, 13936−13941.

8.  Fujita, T.; Takeuchi, Y.; Yamaguchi, K.; Yano, T.; Tanaka, T.; Takeyasu N.; Comparison of hot carrier generation between self-assembled gold and silver nanoparticle arrays tailored to the same hybrid plasmon resonance, *J. Appl. Phys.*   **2020,** *128*, 123104.

9.  Zhang, X.; Li, X.; Zhang, D.; Su, N. Q.; Yang, W.; Everitt, H. O.; Liu, J. Product Selectivity in Plasmonic Photocatalysis for Carbon Dioxide Hydrogenation. *Nat. Commun.* **2017**, *8*, 14542.

10. Zhang, J.; Zhou, R.; Minamimoto, H.; Murakoshi, K. Plasmon- Induced Metal Restructuring and Graphene Oxidation Monitored by Surface-Enhanced Raman Spectroscopy. *Appl. Mater. Today* **2019**, *15*, 372−376.

11. Purcell, E. M.; Pennypacker, C. R. Scattering and Absorption of Light by Nonspherical Dielectric Grains. *Astrophys. J.* **1973**, *186*, 705−714.

12. Rakić, A. D.; Djurišić, A. B.; Elazar, J. M.; Majewski, M. L., Optical properties of metallic films for vertical-cavity optoelectronic devices. *Appl. Opt.* **1998**, *37*, 5271−5283.

13. Saleh, N. M.; Aziz, A. A. Simulation of Surface Plasmon Resonance on Different Size of a Single Gold Nanoparticle. *J. Phys.: Conf. Ser.* **2018**, *1083*, 012041.

# Chapter 4
## Linkages of AuNPs dispersed in solutions

### 4.1　Introduction

Comparison of SEM images of fixed AuNPs revealed that AuNPs were linked by plasmon-induced gold ion reductions. It was also found that the reduction was site-selective due to the distribution of the localized electric field intensity formed during the light illumination. It indicated that the reduction was induced by the light localized at the surface of AuNPs. The linking the metallic nanoparticles provides more complex three-dimensional structures, which is different from geometrical transformation of single nanoparticles. The linkage method can be applicable to strengthen the structures composed of multiple nanoparticles, which is advantageous for the practical use of self-assembled nanoparticles. It is able to form, for instance, AuNP dimers by using the hydrophobic bond in the aqueous solution. The strength of the bond is dependent on the solvent, and thus, it decreases by even replacing water with ethanol. Linkage of AuNPs with metal transforms AuNP dimer to rigid AuND whose geometry is independent of circumstances.

The method can be useful to fabricate the concavity in metal nanoparticles. It was reported that the resonances were dependent on the width of the concavity, which the unique optical property is caused by charge transfer plasmon (CTP).[1] Grzelczak *et al.* have reported the fabrication of Au nanodumbbells (AuNDs), which is the simplest concavity metal nanoparitcle.[2] In the fabrication, gold ions are preferentially reduced at both ends of gold nanorods (AuNRs) in the presence of iodide ions. The longitudinal plasmon resonance was tunable by decreasing the relative thickness of the handle. Xie *et al.* have also reported the conversion of AuNRs to AuNDs by selective transverse etching the tips of AuNRs using $HAuCl_4$.[3] In both methods, the thickness of the handle is dependent on the seed AuNRs, leading to a few ten nanometers thickness. Here, it can be expected that the linkages of metal nanoparticles observed in the last chapter are applicable to the fabricate of the metal nanostructures with thin concavity.

In this chapter, the linkage method was applied to fabricate the AuNDs and other concavity structures. The linkages of AuNP oligomers dispersed in the solution were

performed by the light illumination with a lamp in the presence of gold ions. The concavity (gold bridge) in the linked AuNPs were directly observed with a high-resolution transmission electron microscopy (TEM). The widths of the bridges were also compared with different illumination times. The extinction spectra of illuminated AuNP oligomer solution were measured to observe the spectral transitions due to the linkages.

## 4.2 Experiment

### 4.2.1 Materials and Equipment

For preparation of AuNPs, gold(III) sodium chloride dihydrate ($NaAuCl_4 \cdot 2H_2O$, guaranteed reagent, 98.0%) and tri-sodium citrate dihydrate (extra pure reagent, 99.0%) were purchased from nacalai tesque. 3-Aminopropyldimethoxymethylsilane (97.0%) obtained from Tokyo Chemical Industry Co., Ltd. and ethanol (99.5%) was purchased from nacalai tesque for direct observation of AuNPs. Sodium chloride (NaCl, 99.5%) was obtained from Wako Pure Chemical Industries, Ltd. for aggregation of AuNPs. In order to induce reduction of gold ions, a fluorescent lamp (LOVEEYE, Matsushita Electric Industrial Co., Ltd. ) was used. The extinction spectrum of linked AuNPs was measured by spectrophotometer (UV-3600, SHIMADZU) and AuNP oligomer and linked AuNPs were directly observed by a high-resolution TEM (JEM-2100F/SP, JEOL. Ltd.). EDS mounted on the TEM was used for elemental analysis of linked AuNPs. Yields and the geometries of each AuNP monomer and oligomer were directly observed by a scanning electron microscope (SEM, SU8010, HITACHI).

### 4.2.2 Preparation of AuNP aqueous solution containing AuNP oligomers

An AuNP aqueous solution was prepared by heating the mixture of $NaAuCl_4$ and sodium citrate in water at 80 °C for 3 hours. AuNPs were aggregated by adding NaCl aqueous solution (160 mM) into the prepared AuNP aqueous solution and the resulting solution was left for 1 hour. The volume ratio between the NaCl solution and the AuNP solution was 1:9, resulting in the 16 mM of NaCl in the mixture. In order to prevent AuNPs from excess aggregation, solvent (99%) of the AuNP solution was replaced with ultrapure water after the AuNPs were settled down to the bottom of the tube by centrifugation with 14000×g for 30 minutes. By further centrifugation of the solution at 500×g for 10 minutes and residual AuNP solution (99%) were transferred to other tubes, extremely large AuNP aggregates (> 1 μm) were removed from the AuNP solution. For linkages of AuNPs dispersed in the solution, gold ion aqueous solution (5 mM, 20 μL) and ultrapure water (30 μL) were added to prepared AuNP aqueous solution (4.95 mL) to set the concentration of gold ions 20 μM. Light illumination was performed for the AuNP solution containing gold ions with the fluorescent lamp.

### 4.2.3 Direct observation of AuNP dimers and linked AuNPs with TEM

In order to directly observe the geometry of linked AuNPs, a high-resolution TEM was used. The accelerating voltage was 200 kV. The resolution was 0.23 nm. As a TEM grid, copper grids covered by carbon films (ELS-C10, Okenshoji Co., Ltd.) were used. The TEM observation was performed for the AuNP oligomers and linked AuNPs with different illumination time. Elemental analysis of AuNDs was also performed using EDS mounted on the TEM to confirm the gold bridged in linked AuNPs.

### 4.2.4 Simulation of extinction spectra for AuNP dimer and linked AuNP dimers

For the evaluation of correlation between geometrical variation and transformation of experimentally observed extinction spectra, the extinction spectra were simulated by DDA.[4] The optical properties of each point dipole were given by Ref. 5. As model structure for simulation of AuNP dimer and linked AuNPs, the diameter, gap distance and bridge thickness of linked AuNPs were obtained from TEM images.

### 4.2.5 Aggregation of AuNPs dependence on concentration of NaCl

In order to prepare the AuNP solution with high concentration and ratio of the oligomers, the dependence of NaCl concentration on aggregation of AuNPs was investigated. Solvent (99.9%) of AuNP aqueous solution was replaced with ultrapure water by centrifugation to decrease the concentration of residual citrates in the solution. The cleaned AuNP aqueous solution was used to investigate the dependence. AuNP oligomers were prepared by adding NaCl aqueous solution (1 M) to the cleaned AuNP solution. The concentration of NaCl in the mixture was controlled by varying the volume ratio between NaCl solution and AuNP solution, where the total volume of each mixture was set to 5 mL. By observing the color of each solution, the amount of AuNP oligomers were evaluated. Each color was observed 12 hours later after mixing the AuNP solution and the NaCl solution. At first, the concentration of NaCl was roughly changed, 100, 50, 40, 30, 20, 10, 5 mM, to find the concentration inducing the precipitation of AuNP aggregates. After that, the concentration was changed precisely around the one that AuNPs started aggregating.

### 4.2.6 Preparation of AuNP oligomers dispersed in mixture of water, ethanol, and salts

An AuNP aqueous solution was prepared by the heating mixture of water, trisodium citrate and $NaAuCl_4$ for 3 hours. The solvent of the AuNP aqueous solution was replaced with ultrapure water to decrease the number of residual citrates in the solution. AuNP oligomers were prepared by adding ethanol and salts (NaCl or $NaAuCl_4$) to the cleaned AuNP aqueous solution as referred to 6. The yield of each oligomer was controlled by varying the concentration of salt and volume ratio between water and ethanol.

### 4.2.7 Linkage of AuNP oligomers dispersed in water-ethanol mixed solution by light illumination

Prepared AuNP oligomers were linked by the illumination with the fluorescent lamp. The yields of the monomer and oligomers were confirmed by the SEM images. Prepared or illuminated AuNPs were fixed on amino-coated glass substrates to obtain accurate yields because the AuNPs should be aggregated by the evaporation of solvent due to the neutralized surface charge of AuNPs and disappearance of repulsion force between AuNPs. Each yield was estimated by averaging the yields at randomly selected six observation spots. The optical property of the illuminated sample was investigated by the measurements of the extinction spectrum.

## 4.3  Results and Discussion

### 4.3.1  Direct observation of AuNP dimers and linked AuNPs with TEM

The prepared AuNP oligomers and illuminated AuNPs were directly observed using high-resolution TEM. Figure 4-1 shows the TEM images of the prepared AuNP dimer and illuminated AuNP dimers in the presence of gold ions to compare the geometry between AuNP dimers before and after light illumination. The TEM images of the AuNP dimer prepared by the addition of NaCl revealed that each dimer has spatial gaps between nanoparticles with ~ 1 nm distance. For the AuNPs illuminated by 2 hours, it was found that the colors of gaps were different from the background, indicating linkages of AuNP dimers in the solution. The thickness of observed linkage part was less than 5 nm. In the images of the AuNP aqueous solution illuminated by 4 hours, the dimers were obviously linked, and the thickness was comparable with the radius of composing AuNPs, indicating growth of the linkage part. At 6 hours of illumination, some dimers were finally converted to AuNRs by terminated growth of the linkage part. The results imply that the thickness of the linkage part can be precisely controlled by using plasmon induced chemical reactions.
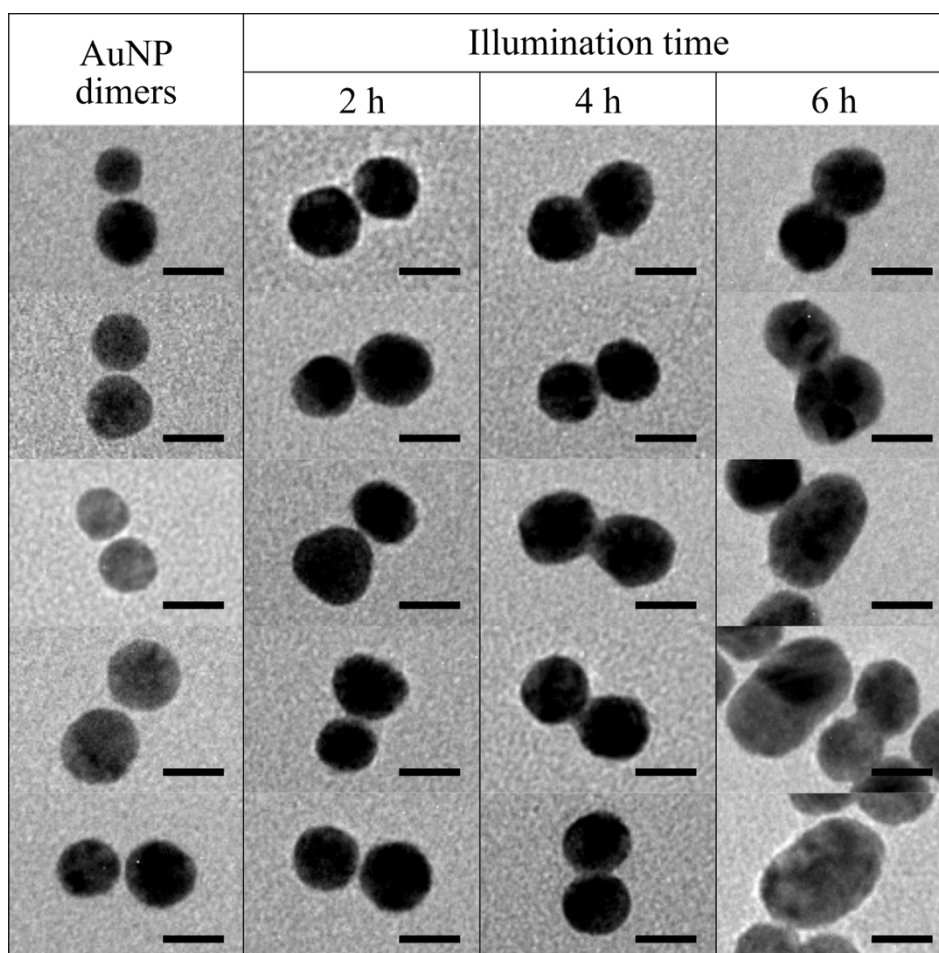
Figure 4-1. TEM images of AuNP dimers and linked AuNPs. The images of linked AuNPs were captured with different illumination time (2, 4, 6 hours). The scale bar is 10 nm for each image.

### 4.3.2 Elemental analysis of linked AuNPs using EDS

The elemental analysis of the linked AuNPs was performed by using an energy dispersive X-ray spectrometer (EDS) mounted on the TEM. Figure 4-2 (a) shows the EDS spectrum of AuNPs illuminated by 4 hours observed in the scanning TEM image displayed in Fig. 4-2 (b). The peaks were assigned as carbon Kα (0.27 keV), oxygen Kα (0.52 keV), copper Kα (8.12 keV), silicon Kα (1.75 keV), and gold Mα (2.13 keV). Except for gold, all elements might be derived from TEM grid and environmental conditions during the measurement of the spectrum. The plot of the X-ray intensity from gold was obtained according to a red line drawn in the scanning TEM image of the linked AuNP as shown in Fig. 4-2 (b). It seems that the plot corresponds to the linked AuNP. The intensity at the linkage part was weaker than the center of each composing AuNP.

As the reason to make the dip of intensity, two possibilities can be considered. One possibility is that the X-ray from the linkage part (gold bridge) was successfully measured, and the intensity is relatively weak because the thickness of the bridge was smaller than the diameters of each AuNP. The other one is that the X-ray emitted from AuNPs adjacent to the linkage part was measured due to the low resolution. In order to confirm the reason for the dip, line-scan measurement was performed as shown in Fig. 4-2 (c). The AuNP was scanned according to the red line in the scanning TEM image, where the line was not overlapped with the linkage part. The plot of the intensity from gold corresponds to the illuminated nanoparticle and the intensity much decreased at the gap, which describes that it is hard to detect X-ray emitted from adjacent Au nanostructure. Therefore, it can be concluded that the AuNPs were bridged by gold because of the plasmon-induced gold ion reduction. Furthermore, it was found that the bridges formed by 2 hours of light illumination were thinner than the bridges formed by methods proposed elsewhere.[7-9]
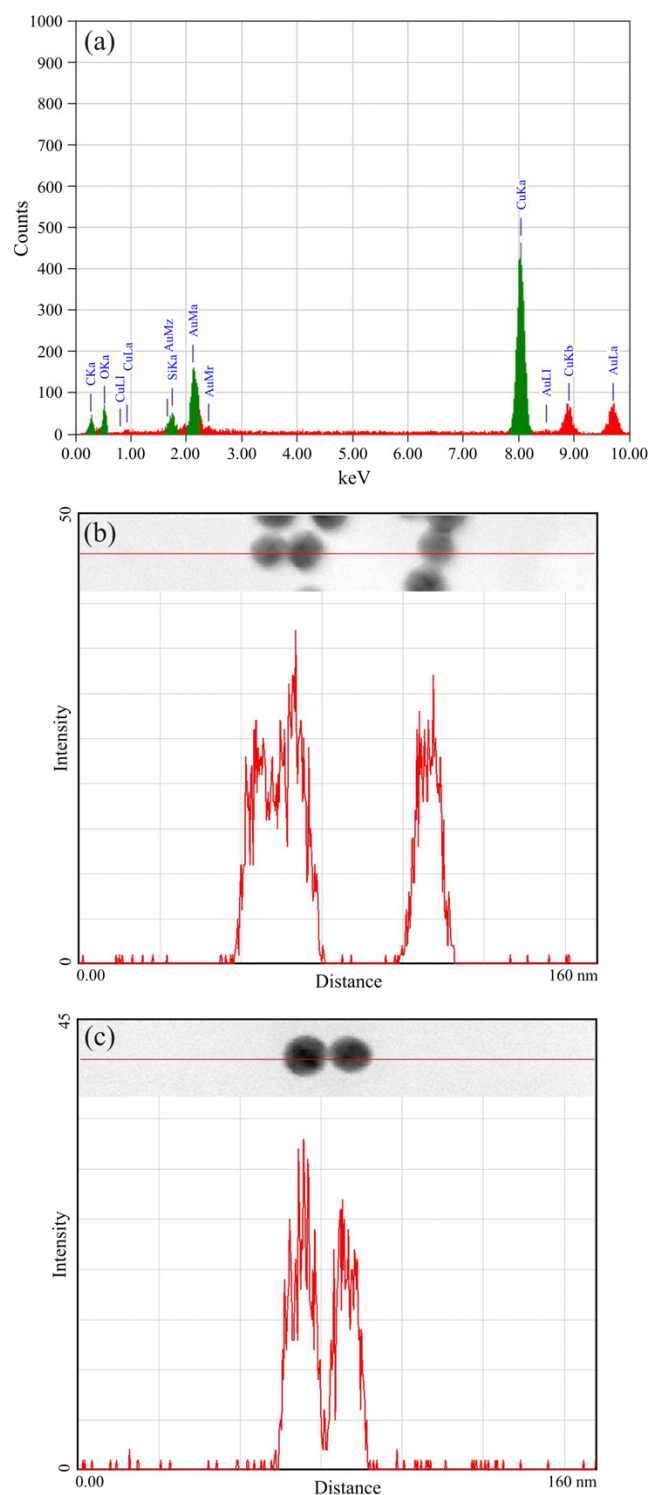
Figure 4-2. (a) EDS spectrum of linked AuNPs observed in scanning TEM image displayed in Fig. 3-2 (b). Scanning TEM image of linked AuNPs and the EDS spectra obtained by line scan when the scan was performed (b) on the bridge or (c) out of the bridge. The scan resolution is ~ 1 nm.

### 4.3.3 Correlation between shape of extinction spectrum and geometry of linked AuNPs

Figure 4-3 (a) shows the extinction spectra of an AuNP solution. All spectra were normalized by each plasmon peak ranging from ~520 to ~530 nm. For AuNPs dispersed in a NaCl aqueous solution, a broad shoulder was observed at the longer wavelength of the peak although the extinction peak was observed, similarly to AuNP aqueous solution, at 521 nm. NaAuCl$_4$ aqueous solution was added to the AuNP aqueous solution so that the concentration of gold ions was 20 μM. The prepared solution was illuminated with the fluorescent lamp. Those extinction spectra were also shown in Fig. 4-3 (a) for each illumination time. After the 2-hour illumination, the extinction peak was slightly red-shifted and the intensity of extinction increased at both longer and shorter wavelengths of the peak, compared to the spectrum of the AuNP aqueous solution before the addition of gold ions. For the spectrum from 4 hours of illumination, the intensity was slightly decreased at near-infrared (NIR) regions and the peak was broadened at ~530 nm. Finally, the intensity further decreased at NIR regions, and the width of the peak also decreased by 6 hours of illumination. The spectral changes should be caused by geometrical change of AuNPs during the light illumination because the optical property is dependent on the geometries of AuNPs.

The changes in spectral shape should be explained by linkages of AuNP oligomers such as the dimer and growth of the bridges. In order to investigate correlation between the spectral changes and the geometrical modifications, the extinction spectra of AuNP dimers and the bridged dimers were simulated by DDA. The calculation model is shown in Fig. 4-3 (b). The gap distance of the AuNP dimer was set to 1 nm, obtained from captured TEM images and the length of the long axis of each dimer was equalized. Figure 4-3 (c) shows the extinction spectra of different structures when the diameter (*d*) is 10 nm. The incident polarization vector is parallel and vertical to the long axis of each structure. In the spectrum of the dimer, the peak was obtained at ~550 nm drawn by a dashed line. On the other hand, the resonance wavelength of AuND with 6 nm of the bridge thickness (*w*) was ~ 800 nm, which indicates that the resonance peak of dimer was largely red-shifted to the NIR region when dimer is linked. Furthermore, the simulation results showed that the resonance peak was blue-shifted by growth of the bridges from

the extinction spectra of bridged dimers with different thickness of bridges ($w = 6$, 8 and 10 nm). The red-/blue-shift of the resonance peak should be observed for the larger oligomers such as AuNP trimer. Such peak shifts by the linkages and growth of formed bridges might be observed in the obtained experimental results of extinction spectra in Fig. 4-3 (a). The red-shift of the resonance peak of the prepared AuNP solution and the increasing intensity at NIR reflects the linkages of AuNP oligomers. It was considered that the increase of broad extinction at NIR was due to a wide variety of thicknesses of the bridges formed between AuNPs. The broad extinction decreased at 4 hours of illumination, which was caused by blue-shifting the resonance of linked AuNP oligomers due to the growth of the bridges in the oligomers. Finally, the further growth and terminated growth of bridges led to the decreasing intensity at NIR region and width of peak as observed in the spectrum of 6 hours illuminated solution.

The peak shift was also confirmed for larger AuNPs ($d = 20$ nm), as shown in Fig. 4-3 (d). Similarly, the extinction peak of the dimer was red-shifted to the NIR region when the dimer was linked. The peak was also blue-shifted by increasing the thickness of the bridge. Furthermore, it was found that the resonance wavelength of AuND was almost the same when the ratio between the diameter of AuNPs and the thickness of the bridge was the same although the diameter is different by comparing the Fig. 4-3 (c) and (d), which implies that the ratio between the diameter and the thickness of the bridge determines the resonance wavelength. Therefore, it can be considered that the change in the spectral shape is also observed in the AuNP solution with the dispersion of diameters, similarly to the simulated single AuNP dimer.

Although the changes in the spectral shape were observed according to the linkages of AuNP oligomers and subsequent growth of formed bridges, the spectra did not show any peaks at NIR regions observed in calculation results of linked AuNPs. As the reasons, the dispersions of the thickness of formed bridges between AuNPs, diameters of composing AuNPs and number of composing AuNPs can be considered. The reduction rate should be determined by the intensity of the electric field formed between the AuNPs, which depends on the diameter of the AuNPs and the distance between the particles. Therefore, variation of the reduction rates was caused by the dispersion of the field intensity, resulting in variations in the thickness of the bridges and dispersion of resonances. The

modulation of resonances is further complicated due to the ratio between thickness of the bridges and diameters of composing AuNPs as predicted by the theoretical method (Fig.4-3c and d). There is dispersion also in the number of AuNPs composing each oligomer, which may lead to additional broadening peaks because the resonance is also dependent on the length of linked AuNPs.

In the experimentally obtained spectra, it seems that the increasing and decreasing intensity of extinction is not apparent at NIR regions. On the other hand, the peak intensity is relatively higher than the extinction at NIR. Although the peak was shifted during the light illumination, the amount of shift was small, indicating the peak dominantly reflects the spectral information of AuNP monomer. Thus, it can be considered that the prepared solution was dominated by AuNP monomers. The previous reports support the consideration, where the dual-peaks were observed for AuNP aggregates dominating solution.[10] The peaks were assigned to hybridized LSPR modes. The hybridization occurs when the interparticle distance is short to induce the near-field interaction between metal nanostructures, in other words, formation of AuNP oligomers such as dimer.[11-13] In the spectra, only one distinct peak is observed, while the low intensity shoulder is also conceded. The spectral shape also shows that the AuNP monomer is dominant in the solution. Therefore, it was concluded that the increasing and small amount of change in intensity was caused because the number of AuNP oligomers was relatively much smaller in the prepared solution.
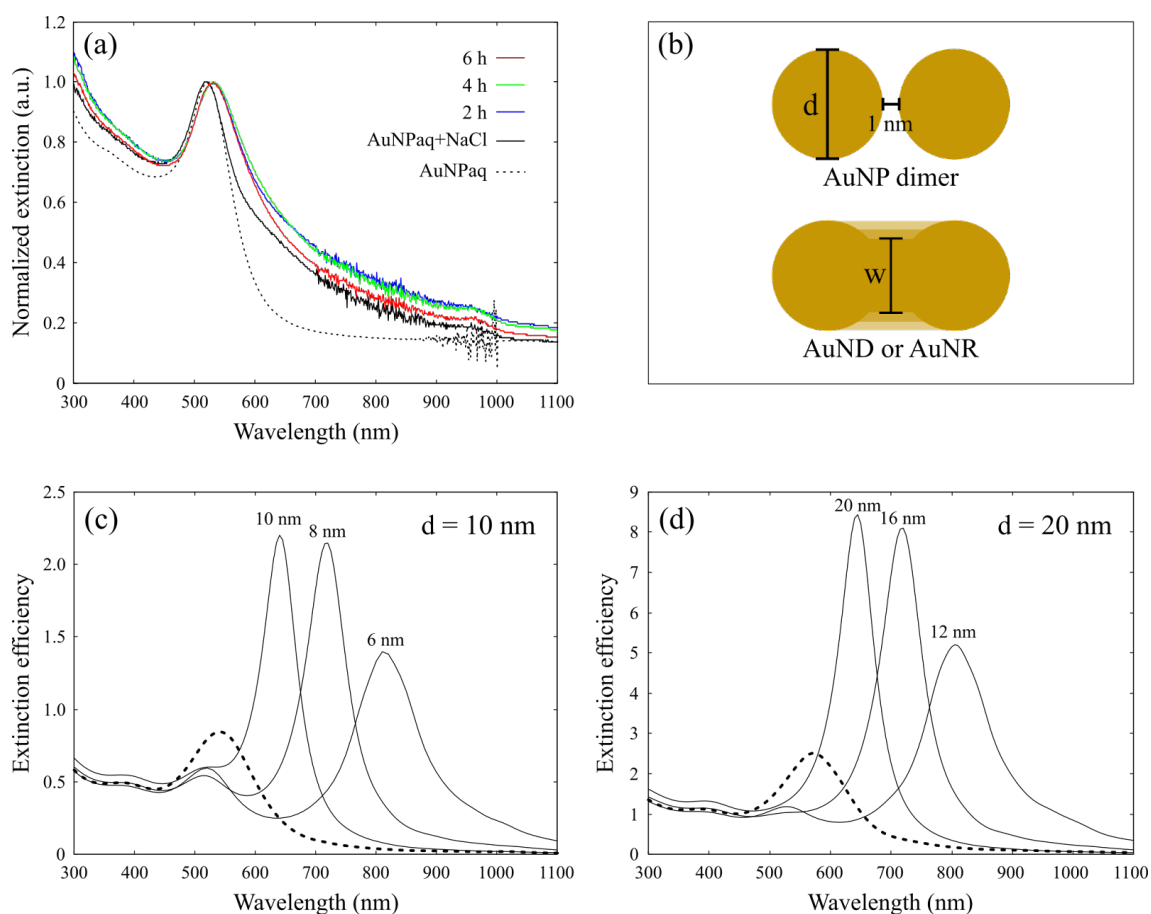
Figure 4-3. (a) Normalized extinction spectra of AuNP solutions. The measurements were carried out for AuNP aqueous solution (dashed black line), the mixture of AuNP solution and NaCl (solid black line) and illuminated the mixture of AuNP solution, NaCl and NaAuCl$_4$. The illumination times were 2 hours (blue), 4 hours (green) and 6 hours (red), respectively. (b) Model of AuNP dimer and linked AuNPs (AuND and AuNR) for simulation. The gap distance of the dimer was 1 nm. The extinction spectra were calculated by changing the diameter ($d$) of each AuNP and thickness ($w$) of the bridge. The length of each long axis of AuND or AuNR was equal to that of the dimer. Simulated extinction spectra of each structure, the dimer, dumbbell, and rod when the diameter of AuNP is (c) 10 nm or (d) 20 nm. The thickness of each bridge was described above each peak in the spectra.

### 4.3.4 Aggregation of AuNPs dependence on concentration of NaCl

The TEM images and EDS spectra represented AuNPs were linked by the gold bridge formed by plasmon-induced gold ion reduction. In the calculation results, the peak of the dimer was shifted to the NIR region by the linkages and the peak was subsequently blue-shifted due to the growth of the bridges. However, the experimentally obtained extinction spectra were not changed widely, especially at NIR regions although the spectral transformation during the light illumination was observed. As the reason, it can be considered that the amount of linked AuNPs were too small to give the signal clearly detected by the spectrophotometer. Furthermore, the concentration of linked AuNPs was relatively much lower than that of the monomer. Therefore, the spectral information of the oligomers is hidden by that of monomers.

In order to obtain the oligomer dominant solution for the observation of spectral information from linked AuNP, aggregation of AuNPs depending on the concentration of NaCl was investigated. First, the change in color of AuNP solution was observed by adding NaCl, resulting in the final concentration of 100, 50, 40, 30, 20, 10, 5 mM. After 12 hours, the solution became transparent at the concentration of NaCl larger than 40 mM although the photograph of each sample was not displayed. In order to find the concentration to initiate excess aggregation of AuNPs more precisely, the color change was also investigated at the final concentrations of NaCl in the AuNP aqueous of 32, 30 and 28 mM, as summarized in Table 4-1. The change in color of the AuNP aqueous by adding different initial concentrations of NaCl aqueous was also compared by using 0.1 M and 1.0 M of NaCl aqueous solution. For 32 mM of NaCl in AuNP solution, the color of both solutions with different initial concentration of NaCl were almost vanished and clear since most of AuNPs were aggregated and precipitated at the bottom of the vial. At 30 mM prepared by 0.1 M of NaCl aqueous solution, it seemed that a larger number of AuNPs remained, but the color is reddish, indicating the monomers are still dominant. Although the color of the 30 mM solution prepared by the 1.0 M of NaCl solution was reddish purple, the color was much diluted. Therefore, it seemed that it was hard to guarantee the strong intensity in the solution. On the other hand, AuNP solution with 28 mM of NaCl showed opaque red for both initial concentrations (0.1 M and 1.0 M) of

NaCl. The result implied that it was difficult to obtain sufficient concentration of AuNP oligomers by adding only NaCl.
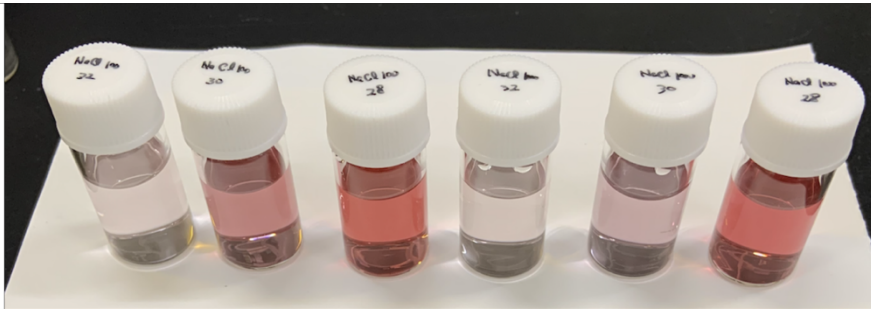
| Photos of AuNPaq containing NaCl with the concentration described below |  | | | | | |
|---|---|---|---|---|---|---|
| Concentration of NaCl for aggregation | 0.1 M | | | 1.0 M | | |
| Amount of NaCl (mL) | 1.28 | 1.20 | 1.12 | 0.128 | 0.120 | 0.112 |
| Amount of AuNPaq (mL) | 2.72 | 2.80 | 2.88 | 3.872 | 3.880 | 3.888 |
| Final concentration of NaCl (mM) | 32 | 30 | 28 | 32 | 30 | 28 |

Table 4-1. Color change of AuNP aqueous solution by adding NaCl. The color was captured when the concentrations of NaCl in the solution were 32, 30 and 28 mM, respectively. In order to compare the effect of initial concentration of NaCl for the aggregation of AuNPs, color changes were observed at both initial concentrations of 0.1 M and 1.0 M, respectively.

### 4.3.5 Preparation of AuNP oligomers and evaluation of the yields of each structure

Because it was difficult to obtain sufficient concentration of AuNP oligomers by adding only NaCl, an alternative method to prepare AuNP oligomer solution was employed. In the method, the oligomers were prepared by adding ethanol and NaAuCl$_4$ into AuNP aqueous solution.[6] Figure 4-4 (a) shows the extinction spectrum of AuNPs dispersed in a water-ethanol mixed solution with 8 μM of NaAuCl$_4$, where the volume ratio of water was 1.8%. The spectrum shows two peaks at ~520 nm and 600 nm derived from the hybridized LSPR modes. The modes can be formed when the gap distances among more than two plasmonic nanoparticles are short, in other words, the nanoparticles are assembled. Therefore, it can be considered that the AuNP oligomers were formed.

In order to elucidate correlation between the spectrum and the obtained structure of AuNPs, the SEM image of AuNPs fixed on the glass substrate via the amino-group was observed as displayed in Fig. 4-4 (b). From the image, the formation of a lot of AuNP oligomers, especially dimer and trimer, were confirmed. Furthermore, it was found that linear oligomer was dominant in the preparation protocol as reported.[6]

The composition ratios of monomer, dimer and larger oligomers were investigated using captured SEM images as shown in Fig. 4-4 (c). I categorized all structures in the sample into three kinds of structures (monomer, dimer, and other oligomers), as shown in the graph. It was found that the dimers (~ 40%) were dominantly produced in the solution although the number of oligomers was larger than the dimer and monomer. The yield of oligomers was counted for all oligomers such as trimer, tetramer and so on. Therefore, the yield of each oligomer can be assumed to be much lower than the dimer, implying that the spectrum of the prepared AuNP solution containing gold ions is dominated by AuNP dimers. The color of the solution was preserved over a few days, indicating that the assembly was terminated in the solution. The AuNP oligomer dominant solution was not achieved in the case of aqueous solution. The stability of AuNPs capped by citrate ions is determined by solvent. The repulsion force is formed between AuNPs due to the deprotonation of citrate ions on AuNPs in the polar solvent such as water and ethanol. The polarity is different among the solvents, for instance, the polarity of water is higher than that of ethanol so that the stability of AuNPs is lower in ethanol, compared to the aqueous solution. Therefore, AuNP oligomers were easily

formed in the water-ethanol mixture, compared to the pure aqueous solution at the same concentration of NaCl, where the surface charge of AuNPs were partially vanished by the effect of ethanol and sodium ions of added NaCl. By partially vanishing surface charges, AuNP chain oligomers were selectively generated at the low concentrations of NaCl. The results are consistent with previous reports.[6]
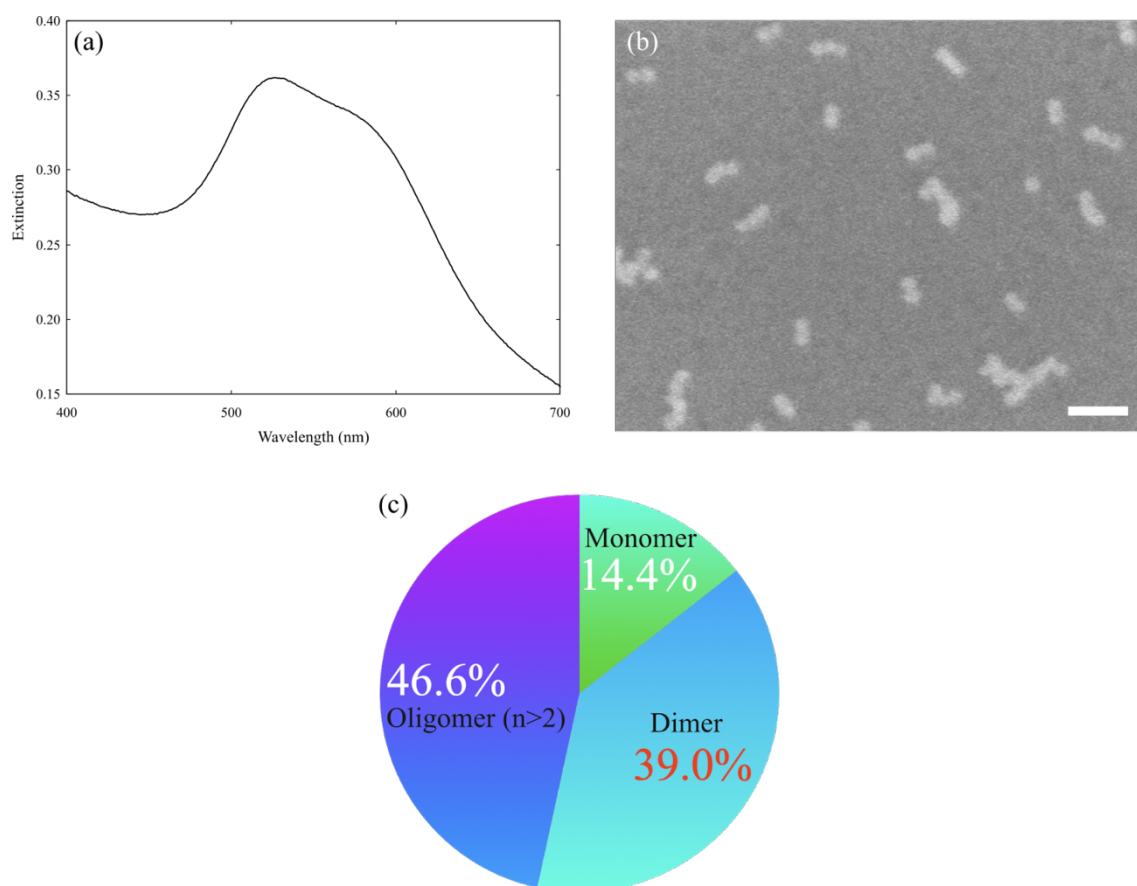


Figure 4-4. (a) Extinction spectrum of prepared AuNP water-ethanol mixed solution containing NaAuCl$_4$. Two peaks are visible in the spectrum. (b) SEM image of AuNP oligomers formed by adding the ethanol and NaAuCl$_4$. AuNPs were fixed onto the glass substrate via the amino group by immersion of amino-coated glass substrate into the prepared AuNP water-ethanol mixed solution to prevent AuNPs from excessive aggregation. The scale bar is 50 nm in the capture. (c) Composition ratio of monomer, dimer, and larger oligomers. It was obtained by counting each structure and averaging the counted numbers in SEM images captured at the randomly selected six observation sites.

### 4.3.6 Illuminating AuNP oligomer solution with 8 μM of NaAuCl₄

The illumination was performed for the prepared AuNP water-ethanol mixed solution with a fluorescent lamp. As shown in Figure 4-5 (a), the modification of the extinction spectrum was tracked for each illumination time. From the comparison of the spectra, it was found that the shape of the spectrum was transformed by the light illumination. For the peak at 520 nm, the height decreased after the light illumination by 2 hours. When the solution was illuminated by 4 hours, the peak grew to be comparable to the peak before the illumination. After 6 hours of illumination, the intensity exceeded the one before the illumination. While the intensity of the peak was varied, the resonance wavelength was not widely shifted. On the other hand, the peak at ~ 600 nm was shifted to longer wavelength regions and the intensity also increased as illumination time.

From the SEM image of AuNPs illuminated for 6 hours (Fig. 4-5b), a lot of AuNP dimers and larger oligomers were observed. It seemed that the gaps of dimer and other oligomers were not filled after the light illumination. The yield was also estimated using the captured SEM images (Fig. 4-5c). By comparing the yields before (Fig. 4-4c) and after (Fig. 4-5c) the illumination, it was found that the rate of each structure in the solution was almost the same. Despite the resonance wavelength being shifted, the gaps filling and changing in the ratio of each structure in the solution were not clearly observed. The reason might be also explained by the gold ion reductions. When the amount of gold ions was not enough to link each AuNP dimer and oligomer in the solution, the linkage process might be stopped before the bridges were formed, which the gap distance became short, compared to the distance before the initiation of the reductions. In Fig. 4-5 (a), the spectrum of AuNP aqueous solution illuminated by 2 hours (blue) might reflect the shortening gap distances. The short gap led to the red-shift of the resonance wavelength of hybridized mode. It was clarified that 8 μM of gold ions was insufficient to link AuNPs.
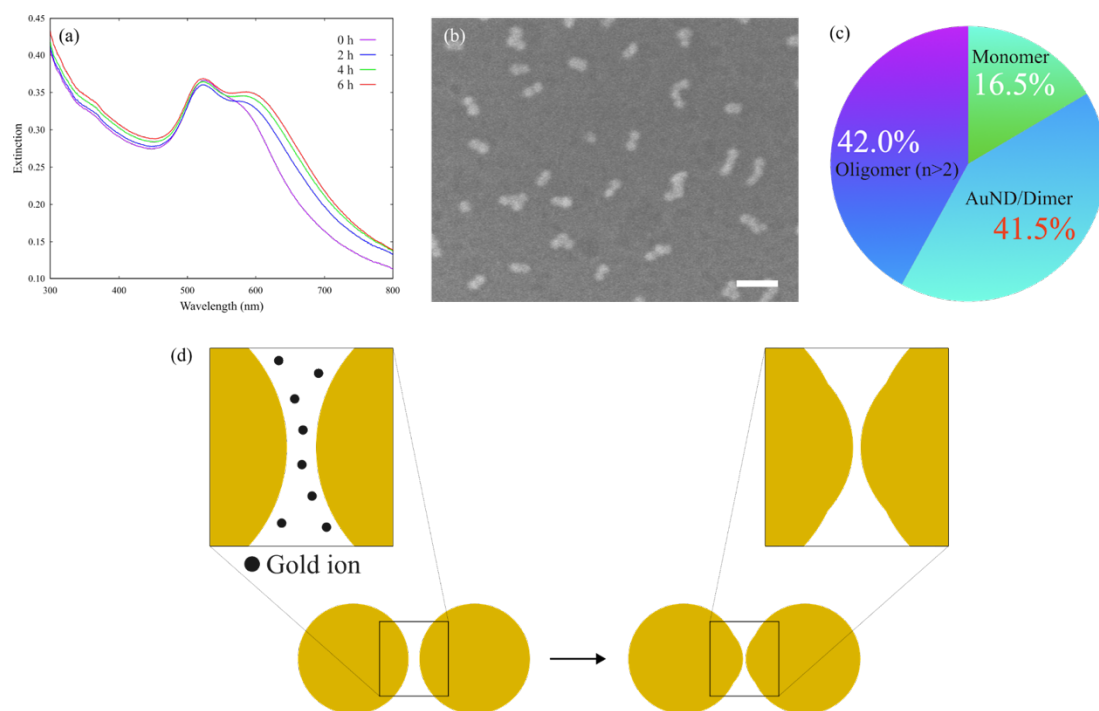
Figure 4-5. (a) Extinction spectra of prepared and illuminated AuNP water-ethanol mixed solution. The color of spectra corresponds to the illumination time of 0 h (purple), 2 h (blue), 4 h (green) and 6 h (red), respectively. (b) SEM image of AuNPs fixed on the amino-coated glass substrate after the illumination for 6 h and the scale bar is 50 nm. (c) The yield of each structure estimated by SEM images. (d) Schematic illustration of shortening the gap distance between AuNPs by the plasmon-induced gold ion reductions.

### 4.3.7 Illuminating AuNP oligomer solution with 80 μM of NaAuCl₄

In order to link all AuNP oligomers, AuNP water-ethanol mixed solution containing 80 μM of NaAuCl₄ with 5% of water was also prepared and illuminated. The extinction spectra were measured for each illumination time. Differently from the spectrum measured in the case of a low concentration of gold ions, the sharp peak derived from AuCl₄⁻ was observed at ~ 310 nm in Fig. 4-6 (a) for the sample solution. Besides the sharp peak due to gold ions, one peak and one shoulder peak were observed at 520 nm and ~ 650 nm, indicating the formation of AuNP oligomers. The shape of the spectrum was transformed after the light illumination for 30 minutes and the sharp peak from gold ions decreased, implying that gold ions were consumed during the light illumination due to the plasmon-induced gold ions reductions. The intensity of the peak at 520 nm increased and the peak at ~ 650 nm was red-shifted to 700 nm accompanied by the consumption of gold ions. The peak was gradually shifted to 900 nm and the peak from gold ions further decreased after 120 minutes of illumination.

The geometry of AuNPs for each illumination time was identified by the SEM observation as summarized in Fig. 4-6 (b). For 30 minutes of illumination, most of the AuNPs were anisotropic with a variety of sizes although the dimers without fully filled gaps remained. The size of AuNPs were grown by the light illumination for 60 minutes. In the capture of the images, a lot of aggregates composed of grown AuNPs were also observed. The growth of AuNPs and those aggregation further occurred, resulting in aggregates ranging from 100 nm to 500 nm for 90 minutes illumination. Finally, the scale reached larger than 1 μm when the solution was illuminated for 120 minutes.

By comparing the AuNP aggregates for each illumination time, it seemed that the size of AuNP was grown anisotropically and the scale of aggregates were also enlarged as increasing the illumination time. The growth of AuNPs and enlargement of aggregates might be caused due to the ethanol environment. The stability of AuNPs were preserved by the capping agent, in this case, citrates. To obtain a lot of AuNP oligomers, the solution consisted of ethanol with 95% and the ethanol might destabilize the AuNPs because the deprotonation of citrate is unfavorable in ethanol, compared to the water solvent, leading to decreasing not only the repulsion force between AuNPs but also the number of citrates covering the surface of AuNPs in the solution. Furthermore, the surface area of AuNPs

were also extended due to the growth of AuNPs by the plasmon-induced gold ion reductions, resulting in increment of the surface uncovered by the citrates. Therefore, the aggregation of AuNPs was promoted due to the extension of the exposed surface in the ethanol-rich solution.

Each spectrum of the illuminated solution has two distinct peaks, implying that the geometries of AuNPs were anisotropic.[14] It is consistent with geometries of AuNPs observed by SEM (Fig. 4-6b). The anisotropic shape of aggregates might be retained because the composing AuNPs produced by linkages during the light illumination were also anisotropic structures. Besides, the aggregates might also be linked by the plasmon-induced gold ion reduction. It also possibly contributed to the redshift of resonance wavelengths.

Through the experiment, it was found that inhibiting the aggregations of AuNPs was necessary although the amount of gold ions was sufficient for the linking.
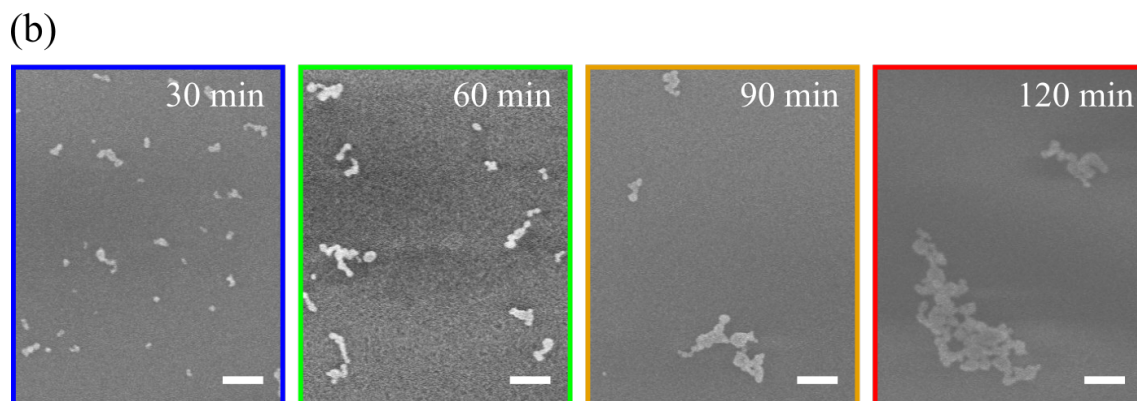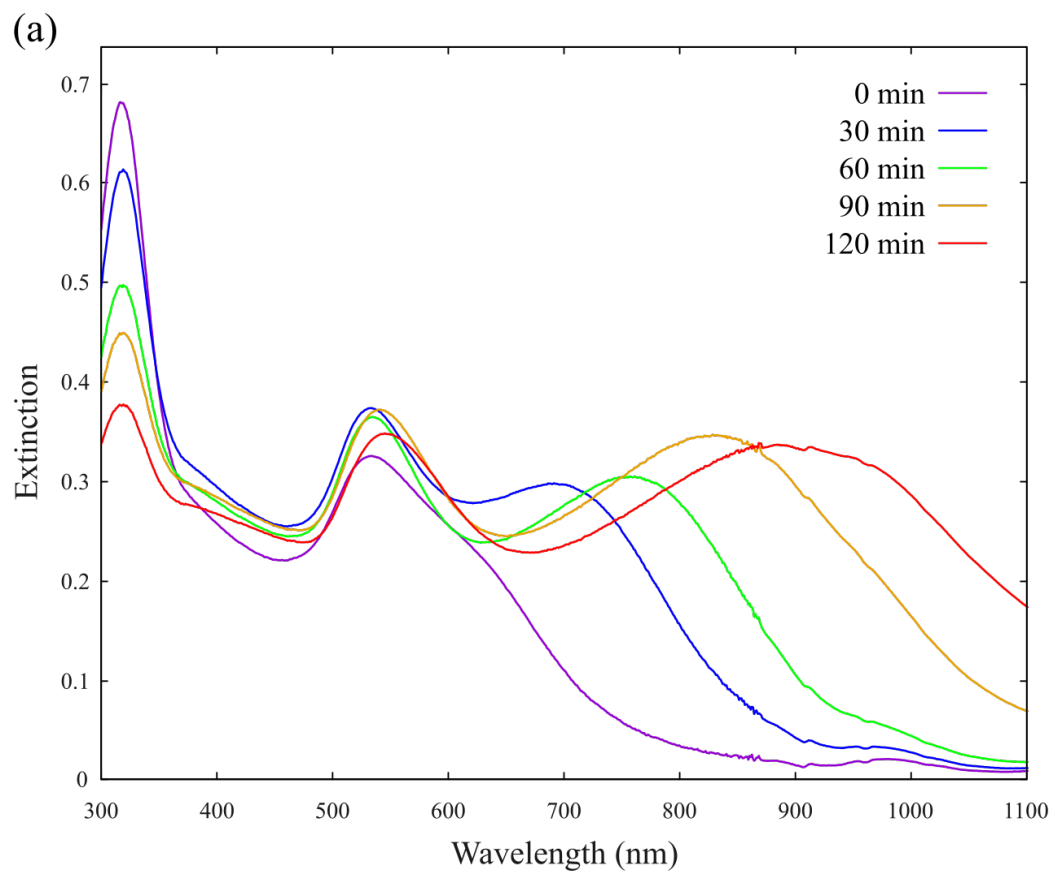
Figure 4-6. (a) Extinction spectra of prepared and illuminated AuNP water-ethanol mixed solution containing 80 μM of $NaAuCl_4$. (b) SEM image of AuNPs fixed on the amino-coated glass substrate for each illumination time. The scale bars are 200 nm in all images. The color of spectra and SEM images corresponds to the illumination time of 0 hours (purple), 30 minutes (blue), 60 minutes (green), 90 minutes (orange) and 120 minutes (red), respectively.

### 4.3.8   Illuminating AuNP oligomer water-rich solution with 100 µM of NaAuCl₄

In order to prevent AuNPs from aggregation during the light illumination, the volume ratio of ethanol in the AuNP solution containing was decreased to 15%. In the preparation of oligomer solution, NaCl was added to AuNP aqueous solution to destabilize the nanoparticles and ethanol was added to the solution, where the concentration of NaCl was 17 mM. By adding $NaAuCl_4$ aqueous solution to the AuNP oligomer solution, the purple color solution was obtained. Figure 4-7 (a) shows the extinction spectrum and the photograph of the prepared AuNP oligomer solution. The sharp peak derived from gold ions was observed at ~ 300 nm. Two peaks from AuNPs were observed at ~ 520 nm and ~ 650 nm, indicating the presence of AuNP oligomers.

The extinction spectra of the AuNP oligomer solution were also monitored with different the illumination time as shown in Fig. 4-7 (b). Similar to the previous experiments, the peak from gold ions decreased by the illumination since gold ions were consumed for the reduction. On the other hand, the transformation of the extinction spectrum was different from the previously obtained results. The peak decreased at 520 nm as the reduction of gold ions progressed. Furthermore, the extinction intensity increased at the NIR range. It seems that the growth of the extinction intensity coincides with the peak decreases at 300 nm and ~520 nm. The change of the spectral shape might be explained by the linkages of AuNP oligomers. By a theoretical method, it was predicted that the intensity of extinction peak decreased and peak was grown at NIR by the linkage of AuNP dimer as shown in Fig.4-3(c,d). The spectral transformation was caused due to the red-shifting of peaks derived from longitudinal mode to NIR regions. Considering the intensity of the extinction peak decreased and the intensity increased at NIR, figure 4-7(b) might reflect the transformation of spectral shape as predicted by the theoretical methods. Therefore, it can be concluded that our observed transformation of the extinction spectrum was also induced by linkages of AuNP oligomers rather than the aggregation of AuNPs during the light illumination.
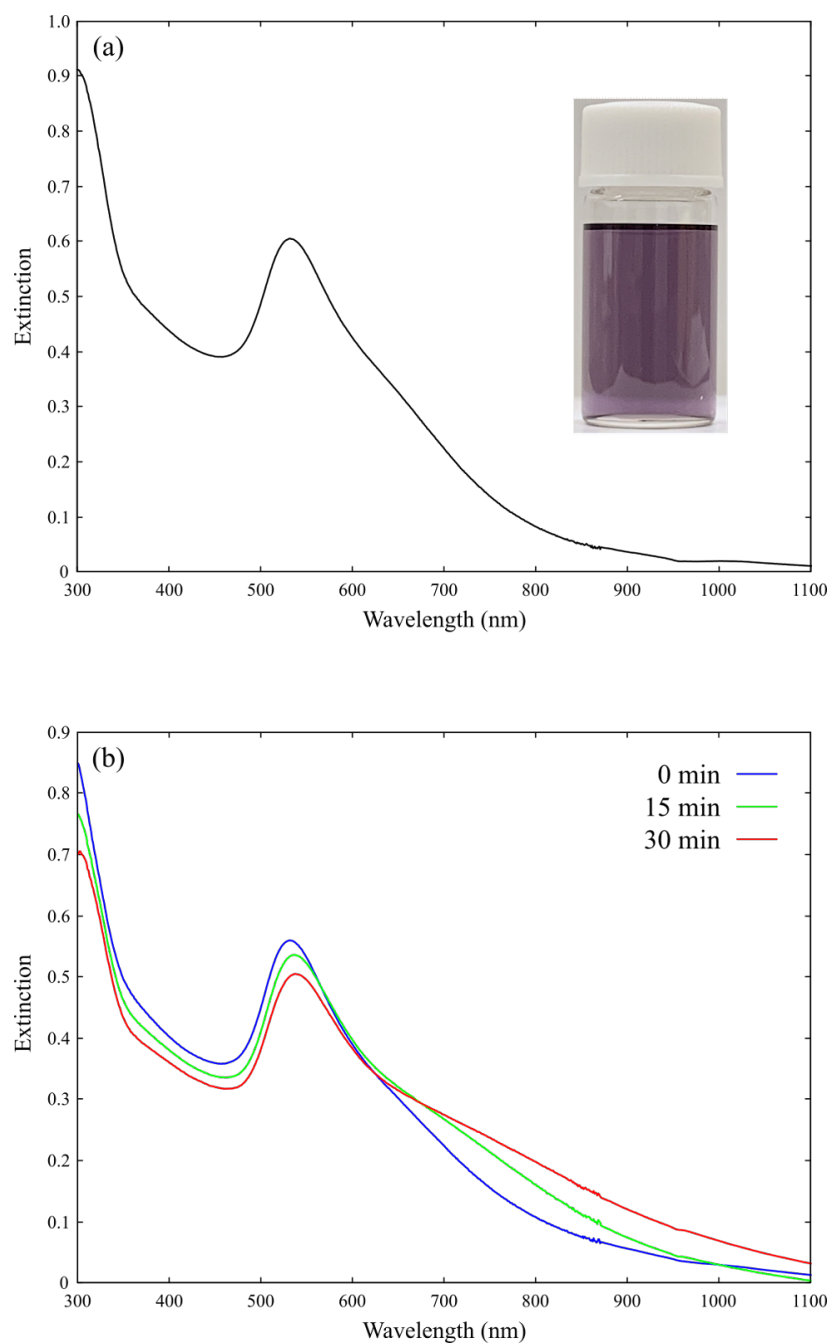
Figure 4-7. (a) Extinction spectrum of AuNP solution prepared by adding ethanol and NaAuCl₄ to AuNP aqueous solution containing NaCl. The concentration of gold ions was 100 μM. The inset shows the photo of the prepared AuNP solution. (b) Illumination time evolution of extinction spectrum of the AuNP solution.

## 4.4　Conclusion

In conclusion, linkage of AuNPs dispersed in the aqueous solution were also confirmed by the measurement of the extinction spectrum and direct observation of those geometry using a high-resolution TEM. The TEM images represented that AuNP oligomers were successfully linked with extremely narrow linkage parts, which the thickness was less than 5 nm. Furthermore, it was found that the thickness was precisely controlled by the illumination time on a few nanometer scales. The elemental analysis of linked AuNPs, especially linkage parts to connect the AuNPs, was also performed by EDS mounted on the TEM. The results showed that the part was composed of gold, indicating the AuNP oligomers were linked by gold bridges formed through the plasmon-induced gold ion reduction. The extinction spectra of linked AuNPs represented that the resonance wavelength was slightly red-shifted and the intensity increased at NIR by linkages of AuNP oligomers, compared to the spectrum of the AuNP solution before the light illumination. The intensity at NIR subsequently decreased, and the peak was broadened, then became sharp due to the growth of formed gold bridges and the termination of growth, resulting in AuNRs. The correlation between the transformation of spectral shape and geometrical change of AuNP oligomers were also supported by calculation results. The peaks were not observed at NIR in experimental results because the resonance of each linked AuNP oligomer were determined by multiple geometrical parameters such as thickness of formed bridges, diameters, and number of composing AuNPs. Although the spectral transformation was observed, the amount of increasing/decreasing intensity of extinction was relatively small, compared to peak intensity at ~520 nm. As the reason, it can be considered that the small number of AuNP oligomers and AuNP monomers dominated in the prepared solution. In order to increase the yield of the oligomers in the solution, the aggregation of AuNPs dependence on the concentration of adding NaCl was investigated. From the results, it was concluded that it is hard to obtain AuNP aqueous solution containing a lot of AuNP oligomers by the addition of only NaCl.

The more stable AuNP oligomer solution was also prepared with the aid of ethanol. The extinction spectrum of the AuNP oligomer solution represents that gold ions were consumed and the resonance wavelength of AuNP oligomers were red-shifted by light illumination. Furthermore, it was found that the geometry was controlled by both the

illumination time and the concentration of gold ions. When the concentration of gold ions was as low as 8 μM, the gap distance became short, and the resonance was slightly red-shifted. The gold bridges were formed by light illumination at the 80 μM of gold ions, showing the red-shift to the NIR region. The red-shift might be induced by not only the linkages of oligomers, but also the aggregation of the linked AuNPs since electrostatically repulsion force was reduced in ethanol. For a AuNP solution with a low rate of ethanol, the peak shrank at 520 nm and the extinction intensity increased at NIR. It might reflect that the longitudinal mode of the small oligomers such as dimer and trimer was red-shifted to the NIR region due to the linkages of the oligomers.

## 4.5 Reference

1. Wen, F.; Zhang, Y.; Gottheim, S.; King, N. S.; Zhang, Y.; Nordlander, P.; Halas, N. J., Charge transfer plasmons: optical frequency conductances and tunable infrared resonances. *ACS Nano* **2015**, *9*, 6428– 6435.

2. Grzelczak, M.; Sánchez-Iglesias, A.; Rodríguez-González, B.; Alvarez-Puebla, R.; Pérez-Juste, J.; Liz-Marzán, L. M., Influence of iodide ions on the growth of gold nanorods: tuning tip curvature and surface plasmon resonance. *Adv. Funct. Mater.* **2008**, *18*, 3780– 3786.

3. Xie, T.; Jing, C.; Ma, W.; Ding, Z. F.; Gross, A. J.; Long, Y. T., Real-time monitoring for the morphological variations of single gold nanorods. *Nanoscale* **2015**, *7*, 511– 517.

4. Purcell, E. M.; Pennypacker, C. R. Scattering and Absorption of Light by Nonspherical Dielectric Grains. *Astrophys. J.* **1973**, *186*, 705−714.

5. Rakić, A. D.; Djurišić, A. B.; Elazar, J. M.; Majewski, M. L., Optical properties of metallic films for vertical-cavity optoelectronic devices. *Appl. Opt.* **1998**, *37*, 5271−5283.

6. Han, X.; Goebl, J.; Lu, Z.; Yin, Y., Role of Salt in the Spontaneous Assembly of Charged Gold Nanoparticles in Ethanol, *Langmuir* **2011**, *27*, 5282-5289.

7. Herrmann, L. O.; Valev, V. K.; Tserkezis, C.; Barnard, J. S.; Kasera, S.; Scherman, O. A.; Aizpurua, J.; Baumberg, J. J. Threading plasmonic nanoparticle strings with light. *Nat. Commun.* **2014**, *5*, 4568.

8. Gonzaĺez-Rubio, G.; Gonzaĺez-Izquierdo, J.; Bañares, L.; Tardajos, G.; Rivera, A.; Altantzis, T.; Bals, S.; Peña-Rodríguez, O.; Guerrero-Martínez,A.; Liz-Marzań, L. M. FemtosecondLaser- Controlled Tip-to-Tip Assembly and Welding of Gold Nanorods. *Nano Lett.* **2015**, *15*, 8282−8288.

9. Fang, L.; Liu, D.; Wang, Y.; Li, Y.; Song, L.; Gong, M.; Li, Y.; Deng, Z. Nanosecond-Laser-Based Charge Transfer Plasmon Engineering of Solution-Assembled Nanodimers. *Nano Lett.* **2018**, *18*, 7014−7020.

10. Zhang, L.; Dai, L.; Rong, Y.; Liu, Z.; Tong, D.; Huang, Y.; Chen, T. Light-Triggered Reversible Self-Assembly of Gold Nano- particle Oligomers for Tunable SERS. *Langmuir* **2015**, *31*, 1164− 1171.

11. Su, K.-H.; Wei, Q.-H.; Zhang, X.; Mock, J.; Smith, D. R.; Schultz, S. Interparticle coupling effects on plasmon resonances of nanogold particles. *Nano Lett.* **2003**, *3*, 1087−1090.

12. Prodan, E.; Nordlander, P. Plasmon Hybridization in Spherical Nanoparticles. *J. Chem. Phys.* **2004**, *120*, 5444−5454.

13. Nordlander, P.; Oubre, C.; Prodan, E.; Li, K.; Stockman, M. I. Plasmon Hybridization in Nanoparticle Dimers. *Nano Lett.* **2004**, *4*, 899−903.

14. Nikoobakht, B.; El-Sayed, M. A., Preparation and Growth Mechanism of Gold Nanorods (NRs) Using Seed-Mediated Growth Method, *Chem. Mater.* **2003**, *15*, 1957–1962.

# Chapter 5
# General conclusion

In this dissertation, the plasmon-induced chemical reaction was investigated in terms of the reactivity, the incident light dependence, and the material dependence. Furthermore, the nanofabrication method was demonstrated using the reaction.

First of all, the surface Raman scattering (SERS) spectra of *p*-toluenethiol (*p*-TT) and 1-butanethiol (1-BT) were measured using silver nanoparticles (AgNPs) 2D arrays. The spectra revealed both *p*-TT and 1-BT were oxidized under the laser irradiation with the excitation wavelength of 532 nm. The reactions might be caused by the active oxygens which were generated at the surface of AgNPs during the excitation of localized surface plasmon resonances (LSPRs). The SERS spectra of *p*-aminothiophenol (*p*-ATP) were also measured by varying the excitation wavelengths (458, 532, 671, and 785 nm) and the laser intensities for evaluation of the incident light dependence. From the results, it was found that the shorter wavelength or higher laser intensity were favorable to induce the dimerization of DMAB, indicating the incident light dependence of the plasmon-induced chemical reaction. The material dependence was further discussed by comparing the reactivity at Au and Ag. The SERS spectra of *p*-ATP showed that the dimerization at Ag was more proceeded, compared to Au, which implied the material dependence of the plasmon-induced chemical reaction.

Next, nanofabrication of metal nanoparticles using the plasmon-induced chemical reaction was demonstrated. AuNPs-fixed glass substrates were immersed into the gold ion aqueous solution and illuminated with a fluorescent lamp. The scanning electron microscope images of AuNPs revealed that the AuNPs were linked by the light illumination. It was considered that the linkages were caused due to the gold ion reductions induced by the light localized at the surface of AuNPs. Furthermore, it was predicted that the resulting geometries were dependent on the transitions of the electric fields formed at the Au nanosurface to promote the reduction of gold ions during the light illumination by theoretical method.

Finally, the linkages of AuNPs dispersed in solutions were also performed. In the experiments, it was confirmed that AuNP oligomers were linked during the light

illumination by high-resolution transmission electron microscopy (TEM). The TEM images also showed that the thickness of the linkage parts to connect AuNPs was less than 5 nm by 2 hours of illumination and the parts were grown during the illumination by a few nanometers scale, indicating that the thickness can be controlled by the illumination time.   The elemental analysis of linked AuNPs were also performed. It revealed that the linkage parts were composed of Au. From the results of the direct observation and elemental analysis, it was concluded that the AuNP oligomers were linked with gold bridges formed through the plasmon-induced gold ion reductions. The transitions of the optical property due to the linkages were discussed based on the extinction spectra. The shape of measured extinction spectra of the AuNP solution were transformed after the light illumination. The simulation results explained that the spectral change was caused by the linkages of AuNPs and subsequent growth of formed bridges. However, the spectral shape was not dramatically changed, especially the intensity at NIR regions because of the low concentration of linked AuNPs in the prepared solution. AuNP solutions containing enough high concentration of the oligomer to provide optical information were prepared with the aid of ethanol. By illuminating the solutions, the shapes of the spectra were dramatically changed. When the concentration of gold ions was low, the ions were exhausted before the AuNPs were linked, leading to the slightly red-shift of the resonance wavelength because the gap distance decreased through the reduction of gold ions. For the high concentration of gold ions, the resonance was widely red-shifted to NIR regions. The red-shift was caused by not only the linkages of AuNP oligomers but also those aggregation because the interparticle repulsion force was decreased due to the protonation of citrates in ethanol and extended surface area by growth of AuNPs. More stable AuNP oligomer solution was prepared by decreasing the volume ratio of ethanol to prevent AuNPs from excess aggregation. The resonance shift of the solution during the light illumination was different from the previously obtained results. The peak decreased at ~ 520 nm and the intensity increased at NIR. The transformation of the spectral shape might reflect the AuNP oligomers exhibiting the resonance at ~ 520 nm were linked, resulting in decreasing the peak intensity due to the shifting of those resonance wavelengths to the NIR region.

## Acknowledgement

## List of publications

### Original papers

1. **Yuki Takeuchi**, Tetsuya Fujita and Nobuyuki Takeyasu,
   "Plasmon-mediated chemical transformation from alkane to alkene on a silver nanoparticle array under 532 nm excitation,"
   Physical Chemistry Chemical Physics, Vol. 21, pp. 7502-7507 (2019).

2. Masahiro Ito, Takashi Ito, Hideyuki Aoki, Koshi Nishioka, Tsugumi Shiokawa, Hiroko Tada, **Yuki Takeuchi**, Nobuyuki Takeyasu, Tadashi Yamamoto, Shogo Takashiba,
   "Isolation and identification of the antimicrobial substance included in tempeh using Rhizopus stolonifer NBRC 30816 for fermentation,"
   International Journal of Food Microbiology, Vol. 325, article number-108645 (2020).

3. **Yuki Takeuchi**, Antoine Violas, Tetsuya Fujita, Yasuaki Kumamoto, Mircea Modreanu, Takuo Tanaka, Katsumasa Fujita and Nobuyuki Takeyasu,
   "Hot Carrier Generation in Two-Dimensional Silver Nanoparticle Array at Different Excitation Wavelengths Under On-Resonant Condition,"
   The Journal of Physical Chemistry C, Vol. 124, No. 25, pp. 13936-13941 (2020).

4. Tetsuya Fujita, **Yuki Takeuchi**, Kenzo Yamaguchi, Taka-aki Yano, Takuo Tanaka and Nobuyuki Takeyasu,
   "Comparison of hot carrier generation between self-assembled gold and silver nanoparticle arrays tailored to the same hybrid plasmon resonance,"
   Journal of Applied Physics, Vol. 128, article number-123104 (2020).

5. Takahiro Ohkubo, Hiroki Nakayasu, Yuki Takeuchi, Nobuyuki Takeyasu, Yasushige Kuroda,
   "Acidic layer-enhanced nanoconfinement of anions in cylindrical pore of single-walled carbon nanotube"

Journal of Colloid and Interface Science, Vol. 629, Part B, pp. 238-244 (2023).

## International Conference

1. **Yuki Takeuchi**, Nobuyuki Takeyasu and Takashi Kaneta,
   "Chemical transformation of *para*-toluenethiol on silver nanoparticle array," MTSA2017-OptoXNano-TeraNano8, no.P-29, (Okayama, Japan, 19th - 23rd, November, 2017). (Poster Presentation)

2. **Yuki Takeuchi**,
   "Reactivity of Hot Carrier Generated by Plasmon,"
   The 3rd OU-SKKU Bilateral Symposium on Photofunctional Materials and Nanointerfaces, (Okayama, Japan, 18th and 25th, November 2019). (Oral Presentation)

3. Tetsuya Fujita, **Yuki Takeuchi**, Kenzo Yamaguchi, Takaaki Yano, Takuo Tanaka, Nobuyuki Takeyasu,
   "Dependence of hot carrier generation on gold and silver under on-resonant condition using nanoparticle 2D arrays,"
   OptoX-NANO 2019, no.P-13, (Okayama, Japan, 2nd - 5th, December, 2019). (Poster Presentation)

4. **Yuki Takeuchi**, Antoine Violas, Tetsuya Fujita, Yasuaki Kumamoto, Mircea Modreanu, Takuo Tanaka, Katsumasa Fujita and Nobuyuki Takeyasu,
   "Dependence of hot carrier-generation on excitation wavelength in the silver nanoparticles,"
   OptoX-NANO 2019, no.TuA4-4S, (Okayama, Japan, 2nd - 5th, December, 2019). (Oral Presentation)

5.  Masahiro Ito, Takashi Ito, Shin Nakamura, Hideyuki Aoki, Koshi Nishioka, Tsugumi Shiokawa, Hiroko Tada, **Yuki Takeuchi**, Nobuyuki Takeyasu, Kazuhiro Omori, Tadashi Yamamoto, Shogo Takashiba,
    "Identification of an antimicrobial substance from soybean fermented "tempeh","
    International Association for Dental Research, (Vancouver, BC, Canada, 19th - 22nd June, 2019). (Poster Presentation)

**Domestic Meeting**

1.  **竹内 祐貴**，武安 伸幸，
    "1－ブタンチオールの SERS 計測中のプラズモン誘起化学反応,"
    応用物理学会，no.20p-224A-15,（愛知，18 日-21 日， 9 月， 2018 年).（口頭発表）

2.  木内 泰治，武安 伸幸，**竹内 祐貴**，花田 修賢，
    "フッ素系ポリマーのプラズモン誘起化学反応,"
    応用物理学会, no.20p-224A-14,（愛知，18 日-21 日， 9 月， 2018 年).（口頭発表）

3.  **Yuki Takeuchi**, Kotaro Mukaiyama, Nobuyuki Takeyasu, Yasutaka Hanada,
    "Multi-photon induced plasmon chemical transformation for laser microfabrication,"
    JSAP-OSA Joint Symposia, no.18a-E208-6, (Hokkaido, Japan, 18th - 21st, September 2019). (Oral Presentation)

4.  藤田 哲也，**竹内 祐貴**, Violas ,Antoine, 熊本 康昭, Modreanu Mircea, 田中 拓男，武安 伸幸，
    "銀ナノ粒子 2 次元アレイを用いたオンレゾナント条件下におけるホットキャリア生成の励起波長依存性,"
    応用物理学会, no.20p-E208-12,（北海道, 18 日-21 日, 9 月, 2019 年).（口頭発表）

5. 向山 光太郎，**竹内 祐貴**，武安 伸幸，花田 修賢，
   "銀ナノ粒子の近接場を用いた紫外透過性ポリマーのナノ加工"，
   応用物理学会, no.14a-PB4-10,（東京, 12 日-15 日, 3 月, 2020 年).（口頭発表）

6. **竹内 祐貴**，田中 拓男， 武安 伸幸，
   "表面プラズモン誘起金属イオン還元よる金ナノ粒子の連結，"
   応用物理学会, no.23a-E303-7,（東京, 22 日-26 日 3 月, 2022 年).（口頭発表）

7. Takashi Takeuchi, Kazuhiro Yabana, Yuki Takeuchi, Takuo Tanaka,
   "Nonlinear Optical Response Analysis of Metallic Nanostructures - A Relationship
   between Electron Spill-out and 3rd-order Optical Nonlinearity,"
   JSAP-Optica-SPP Joint Symposia, no.20p-C304-11, p.04-022, (Miyagi, Japan, 20th
   – 23rd, September 2022). (Oral Presentation)